Rapid and specific degradation of endogenous proteins in mouse models using auxin-inducible degrons

Lewis Macdonald[1*], Gillian Taylor[1*], Jennifer Brisbane[1], Ersi Christodoulou[1], Lucy Scott[1], Alex Von Kriegsheim[2], Janet Rossant[3], Bin Gu[4, 5, 6], Andrew Wood[1]

[1] MRC Human Genetics Unit, Institute of Genetics and Cancer, University of Edinburgh, Edinburgh, EH4 2XU, UK

[2] Cancer Research UK Edinburgh Centre, Institute of Genetics and Cancer, University of Edinburgh, Edinburgh, EH4 2XU, UK

[3] Program in Developmental and Stem Cell Biology, Peter Gilgan Centre for Research and Learning, Hospital for Sick Children, Toronto, Ontario, Canada

[4] Department of Obstetrics, Gynecology and Reproductive Biology, Michigan State University East Lansing, MI 48824, USA

[5] Department of Biomedical Engineering; Michigan State University East Lansing, MI 48824, USA

[6] Institute for Quantitative Health Science and Engineering, Michigan State University East Lansing, MI 48824, USA

* Equal contribution

Requests relating to the Rosa26^{Tir1} mouse allele to Bin Gu (guibin1@msu.edu).

Requests relating to the Ncaph and Ncaph2 AID:Clover alleles and all other correspondence on the manuscript to Andrew Wood (Andrew.j.wood@ed.ac.uk).

Highlights

- **Auxin-inducible degradation of endogenously tagged proteins in living mice and a range of primary cells.**
- **Most but not all cell types are competent for degradation**
- **Dosage of the tagged protein, E3 ligase substrate receptor and ligand can all determine degradation kinetics**
- **Rapid degradation of condensin subunits in lymphocytes reveals stage-specific requirements during cell division**

Abstract

Auxin-inducible degrons are a chemical genetic tool for targeted protein degradation and are widely used to study protein function in cultured mammalian cells. Here, we develop CRISPR-engineered mouse lines that enable rapid and highly specific degradation of tagged endogenous proteins *in vivo*. Most but not all cell types are competent for degradation. Using mouse genetics, we show that degradation kinetics depend upon the dose of the tagged protein, ligand, and the E3 ligase subunit Tir1. Rapid degradation of condensin I and condensin II – two essential regulators of mitotic chromosome structure - revealed that both complexes are individually required for cell division in precursor lymphocytes, but not in their differentiated peripheral lymphocyte derivatives. This generalisable approach provides unprecedented temporal control over the dose of endogenous proteins in mouse models, with implications for studying essential biological pathways and modelling drug activity in mammalian tissues.

Introduction

Methods to conditionally control gene function are an important part of the genetic toolbox in a wide range of experimental model systems. In rodents, conditional approaches typically make use of recombinases such as Cre and Flp, which allow the controlled excision, inversion or translocation of DNA flanked by recombinase target sites [1]. Despite the immense contribution that recombinase-based systems have made to mouse genetics, their utility in studies of protein function is fundamentally limited by the fact that they target DNA.

DNA manipulations impact protein function slowly, with kinetics that are determined by the natural half-life of pre-existing mRNA and protein molecules. Chemical genetic approaches such as the auxin inducible degron (AID) provide a potential solution to these problems[2,3]. Auxins (e.g. indole-3-acetic acid (IAA)) are plant hormones that bind to Tir1, the substrate receptor subunit of a Cullin Ring E3 ubiquitin ligase complex [4]. IAA binding greatly increases the affinity of Tir1 for target proteins containing a degron polypeptide [4], leading to the formation of a ternary complex, ubiquitination of the target protein, followed by its rapid degradation by the proteosome.

Pioneering work by the Kanemaki laboratory showed that this plant-specific system can be co-opted to conditionally degrade target proteins in non-plant species [2,5]. This is achieved by genetically fusing short degron tags (44 amino acids [6,7]) to a protein of interest in cells that heterologously express a plant Tir1 transgene. Addition of IAA ligand then induces rapid degradation of the degron-tagged protein, often with a half-life of less than 30 minutes, in a manner which is both reversible and dosage controllable [2]. Other degron tag systems such as dTAG [8,9], and HaloPROTAC [10] work on a similar conceptual basis, albeit via different molecular mechanisms.

These genetically encoded strategies for targeted protein degradation have revolutionised functional studies of essential proteins in cultured mammalian cells and invertebrates, providing insights into a range of ‘fast’ processes such as transcription [11,12], chromosome looping [6,13] and the cell cycle [14]. However, targeted protein degradation in genetically engineered mammals remains in its infancy [15,16], and it has not yet been possible to degrade tagged endogenous proteins in adult tissues. Such an ability would enable protein function to be compared across a wide range of ‘normal’ cell types and disease models.

In a proof-of-principle study, we (BG, JR) previously observed degradation of transcription factors in early mouse embryos that were mosaic for expression of both Tir1 and the AID-tagged target protein [15]. More recently, a modified AID system (AID2) was shown to induce degradation of a randomly integrated GFP transgene in adult and embryonic mouse tissues following intraperitoneal ligand injection [16]. However, the original and more extensively characterised AID system was not tested in this study due to difficulties in deriving stable mouse lines expressing *Oryza sativa* Tir1.

Here, we derive novel transgenic mouse lines to show that the original AID system is highly effective for acutely depleting endogenously expressed proteins in adult tissues, embryos and primary cells. Using a proteome-wide approach, we show that AID is highly specific for the target protein *in vivo.* Mechanistically, we find that the dosage of Tir1, IAA ligand and the AID-tagged target protein are all key determinants of degradation efficiency in primary cells. We then focus on the two mammalian condensin complexes to show that IAA-responsive mice allow the comparison of 'essential' protein function over short time-scales across cell lineages, and at different stages of differentiation.

Results

Rapid degradation of AID-tagged endogenous proteins in primary cells

The condensin I and II complexes (Figure 1A) are essential for mitotic chromosome formation and chromosome segregation in vertebrate cells [17], and are thought to work via a DNA-dependent motor activity to generate loops in chromosomal DNA [13,18]. AID-tagging of condensin subunits has enabled the consequences of their acute depletion to be studied in various cancer cell lines [13,19,20]. However, it has been challenging to compare the functional requirement for condensins, or indeed other essential proteins, during cell division in different somatic cell lineages.

To address this, we generated mice in which the function of each condensin complex could be perturbed by IAA-mediated targeted proteolysis. The Easi-CRISPR approach [21,22] was used to generate two transgenic lines in which cassettes encoding the mini-auxin-inducible-degron and Clover fluorescent protein (AID:Clover) were fused to the C-terminus of endogenous condensin subunit genes via a short flexible linker peptide (Ncaph$^{AID:Clover}$ & Ncaph2$^{AID:Clover}$, Figure 1A, 1B, Supplemental Methods). The kleisin subunits Ncaph and Ncaph2 were selected for tagging as they are expressed at levels that are limiting for holocomplex assembly (Walther et al 2018), and are known to be essential for condensin complex function in mice [23,24]. Degradation of Ncaph and Ncaph2 should therefore ablate the function of condensin I and II, respectively.

In line with previous studies in cultured cells [13,20,25], C-terminal tagging did not substantially affect steady-state expression (Figure 1C), or localisation to mitotic chromosomes (Figure 1D), for either fusion protein. Mice homozygous for the tagged alleles were born at the expected mendelian frequency from crosses of heterozygous parents (Figure S1A), whereas null mutations in either target gene are known to cause embryonic lethality in the homozygous state [23,24]. Ncaph$^{AID:Clover}$ homozygotes had similar litter sizes (Figure S1B), and were not growth impaired (Figure S1C) compared to heterozygotes, but Ncaph2 homozygotes were less fertile and smaller (Figure S1B, S1C). No other developmental abnormalities were observed in either line, indicating that the essential functions of Ncaph and Ncaph2 are largely retained by the tagged proteins.

In parallel, we generated transgenic animals expressing the *Oryza sativa* (*Os*) *Tir1* gene constitutively by targeting a Tir1 expression construct to the *Rosa26* locus (Figure 1E, Figure S1D) by microinjection of CRISPR-Cas9 reagents and a plasmid

donor into mouse embryos at the two-cell stage [15,26]. Initially, we attempted but failed to generate a mouse line constitutively expressing the *OsTir1* gene at the Rosa26 locus driven by the CAG promoter, consistent with other reports [16]. We reasoned that the transient overexpression of Tir1 from the many copies of injected donor plasmids may have led to non-specific protein degradation in embryos and prevented us from generating live founder pups. We circumvented this hurdle by first generating a single copy insertion of a conditionally activatable Lox-STOP-Lox (LSL) allele (R26-CAG-LSL-TIR1-9myc (Figure S1D)). The R26-CAG-LSL-TIR1-9myc mice were then bred with a constitutive Cre line (pCX-NLS-Cre) to remove the LSL cassette and generate the R26-CAG-TIR1-9myc mouse line (hereafter *Rosa26*^{Tir1}). Western blotting revealed broad expression of Tir1 across tissues (Figure S1E).

In order to generate IAA-responsive mice, we performed crosses to combine the *Rosa26*^{Tir1} allele with either *Ncaph*$^{AID:Clover}$ or *Ncaph2*$^{AID:Clover}$ in double transgenic animals (Figure 1F). The presence of Tir1 has previously been reported to induce 'basal' degradation of some AID tagged target proteins even in the absence of exogenous IAA [16,27,28]. Importantly, the presence of *Rosa26*^{Tir1} alleles had little (Ncaph) or no (Ncaph2) effect on target protein expression (Figure 1G). Accordingly, double homozygotes were obtained at, or greater than, the expected mendelian frequencies from crosses of *Ncaph- or Ncaph2*$^{AID:Clover/AID:Clover}$*; Rosa26*$^{OsTir1/+}$ parents (Figure S1F), and both sexes were fertile (Figure S1G). No significant difference in weight was observed between *Ncaph- or Ncaph2*$^{AID:Clover/AID:Clover}$ animals with 0, 1 or 2 alleles of *Rosa26*^{osTir1} (Figure S1H). Thus, despite low-level affinity of Tir1 for the degron peptide in the absence of auxin [4], we conclude that the *Rosa26*^{osTir1} transgene did not cause biologically significant levels of auxin-independent degradation for either target protein.

The ability of IAA to induce targeted protein degradation was then tested in short term cultures of primary CD8^{+} thymocytes, embryonic fibroblasts and neural stem cells harvested from animals homozygous for either AID-tagged allele in combination with Tir1 (Figure 2A). In each case, addition of IAA to the culture media resulted in near complete (>90%) protein degradation within 2 hours (Figure 2B, 2C, 2D, 2E).

Dosage of ternary complex components determines degradation efficiency

AID and other degron tagging approaches achieve protein degradation through the formation of a ternary complex comprising a ligand, an E3 ligase substrate receptor, and the degron-tagged target protein (Figure 3A, [4]). Complex formation induces ubiquitination of target proteins via an E3 ligase: for the AID system this is SCF^{Tir1}. It is well established that the kinetics of protein degradation are determined, and can be experimentally manipulated by, ligand dose [2,3]. We confirmed this finding in primary neural stem cells derived from *Ncaph*$^{AID:Clover/AID:Clover}$ and *Ncaph2*$^{AID:Clover/AID:Clover}$ animals homozygous for *Rosa26*^{Tir1} (Figure 2E). Whether the kinetics of targeted protein degradation are also controlled by the cellular dosage of the target protein and/or substrate receptor is less well understood.

To address the role of substrate receptor dosage, we compared the efficiency of target protein degradation in primary thymocytes derived from animals with homozygous AID:Clover-tagged Ncaph or Ncaph2 substrate proteins in combination with either 1 or 2 copies of the *Rosa26*^{Tir1} transgene. This analysis revealed that two copies of Tir1 resulted in more efficient degradation of target proteins compared to a single copy (Figure 3B, 3C, 3D). The same trend was observed consistently for both Ncaph and Ncaph2 target proteins (Figure 3B, 3C), in the presence of either one or two AID-tagged alleles (Figure 3B & 3C, Figure S2). Depletion kinetics of mammalian proteins are therefore controlled not only by ligand dose, but also by dosage of the E3 ligase substrate receptor protein Tir1.

To determine the effect of target protein dosage on degradation efficiency, we designed a competition experiment which took advantage of the two distinct AID-tagged alleles that were available. The relative steady-state expression level of tagged Ncaph and Ncaph2 proteins was first quantified by flow cytometric measurement of Clover fluorescence in primary thymocytes. This revealed that the ratio of Ncaph to Ncaph2 is approximately 4.5 : 1 (Figure 4A), which is consistent with previous measurements in HeLa cells [25]. Next, we performed crosses to generate *Ncaph2*$^{AID:mClover/+}$ animals carrying either 0, 1 or 2 alleles of *Ncaph*$^{AID:mClover}$ on a *Rosa26*$^{Tlr1/Tir1}$ background, which allowed us to ask how the degradation kinetics of a constant dose of Ncaph2 protein are affected by the addition of 'decoy' Ncaph proteins at increasingly high dose (Figure 4B & 4C). These experiments confirmed that Ncaph2 degradation was less efficient when the overall quantity of AID-tagged protein increased (Figure 4D & 4E). In summary, dosage of all three

components of the ternary complex can be limiting, and therefore control the degradation kinetics of AID-tagged target proteins.

Comparing essential gene function between primary cell types

Loss of function mutations in condensin subunits cause fully penetrant embryonic lethality in mice [23,24,29], but it is not known whether each complex is absolutely required for cell division throughout development. Our system for rapidly depleting essential condensin I and condensin II subunits in different primary cell types enabled us to address this question. A BrdU-pulse chase assay was established to assess the efficiency of cell division during a single cell cycle across primary cell types.

We chose to focus on lymphocyte development, specifically comparing how rapid degradation of either condensin I or II subunits affected cell division in precursor versus mature cells in both the B and T cell lineages. Explanted cells from the bone marrow (precursor B), thymus (precursor T) or spleen (peripheral B and T – see Methods for cell purification details) were cultured for two hours in the presence or absence of auxin to degrade either Ncaph or Ncaph2, then subjected to a 30 minute BrdU pulse followed by washout and chase (Figure 5A). BrdU and DNA content were then measured by flow cytometry (Figure 5B). Over time, a fraction of $BrdU^+$ cells divide to form G1 daughter cells with 2n DNA content (Figure 5C). If loss of either condensin complex inhibits cell division, IAA treatment should reduce the fraction of $BrdU^+$ cells that progress through mitosis into G1 during the chase (Figure 5D). By quantifying and comparing the extent of this reduction across cell types (Figure 5E), we tested their ability to complete a single cell division in the near absence of condensin I or II. As expected, acute degradation of either Ncaph or Ncaph2 did not affect BrdU incorporation (Figure S3A) or induce marks of DNA damage during S phase (Figure S3B), but instead caused an accumulation of 4N cells (Figure 5D) consistent with a cell cycle block during G2/M.

In primary cells from $Ncaph^{AID:Clover/AID:Clover}$; $Rosa26^{Tlr1/Tir1}$ mice, acute depletion of an essential condensin I subunit impacted cell division to a significantly greater extent in precursor T cells isolated from the thymus compared to activated mature T cells isolated from the spleen (Figure 5D, 5E & 5F). In thymocytes, where most cell division occurs at the 'beta-selection' stage of T cell differentiation [30], treatment caused an 88% reduction (21.6% versus 3.1%, Figure 5E, 5F) in the

fraction of G1 cells among the BrdU$^+$ population following a 3.5 hour chase. In contrast IAA treatment of activated splenic T cells caused only a 22% reduction in this population (39% versus 31% of BrdU$^+$ cells in G1, Figure 5E & 5F). By the same measure, precursor B cells isolated from the bone marrow were significantly more sensitive to Ncaph depletion compared to mature B cells isolated from the spleen (67% versus 48% reduction in BrdU$^+$ G1 cells, respectively, Figure 5E & 5F). The same experiments repeated in primary cells from *Ncaph2*$^{AID:Clover/AID:Clover}$; Rosa26$^{Tir1/Tir1}$ animals revealed similar trends, with precursors more sensitive to condensin perturbation compared to mature cells, albeit with less profound effect sizes.

The observed differences between cell types were not attributable to differences in the extent of protein degradation, which were similar between precursor and peripheral cell populations (Figure S3C). However despite the relatively mild consequences of condensin degradation on peripheral lymphocytes over a single cell division (Figure 5D, 5E & 5F), cell trace experiments still showed a clear impact on proliferation over several cell cycles (Figure S3D). Altogether, these experiments show that lymphocytes at later stages of differentiation are better able to complete a single round of cell division in the near-absence of either condensin I or condensin II compared to their respective precursor cell populations.

Acute degradation of AID-tagged proteins in living mice

Having established the utility of the AID system to compare essential protein functions between primary cell types, we next investigated its use in living adult mice. Because condensin expression is largely restricted to proliferating cells in adult tissues, we initially focused on haematopoietic organs where dividing cells are abundant. In a pilot dose-finding study, adult *Ncaph*$^{AID:Clover/+}$ *Rosa26*$^{Tir1/Tir1}$ mice received a single dose of IAA via intraperitoneal (I.P.) injection, then thymus tissue was collected 2 hours later to quantify Clover fluorescence using flow cytometry. Increasing levels of protein degradation were observed as the dose was increased from 50 to 100 mg kg^{-1} (Figure S4A). All subsequent experiments were therefore performed using the 100 mg kg^{-1} dose. To evaluate hepatic toxicity of IAA, a panel of liver function tests was performed on plasma collected from animals either 2 hours or 72 hours following I.P. injection of IAA or vehicle. No significant differences were observed (Figure S4B).

Adult animals homozygous for AID-tagged kleisin alleles and Tir1 were then injected I.P. with IAA, then haematopoietic organs were collected either 1 or 2 hours post-injection (Figure 6A). Flow cytometric quantification of Clover fluorescence in proliferating thymocytes (Figure 6A) and bone marrow B cell precursors (Figure S4B) revealed that a majority of target protein was typically degraded within 1 hour of injection, and near complete degradation (>90%) was achieved within two hours, although some variability was observed between replicates. To validate knockdown efficiency using an orthogonal method, and to assess the proteome-wide specificity of the AID system, thymus tissue was collected from *Ncaph2*$^{AID:Clover/AID:Clover}$ *Rosa26*$^{Tir1/Tir1}$ animals 2 hours following I.P. injection of IAA or vehicle, and proteomic quantification was performed using mass spectrometry (Figure 6B). This confirmed profound (~10-fold) downregulation of the target protein. Remarkably, no other protein was significantly downregulated using thresholds of $p < 0.01$ and > 2-fold change. Only a single protein (the heat shock protein Hspb11) was significantly upregulated. Relaxing the significance threshold to $p < 0.05$ led to only 3 downregulated proteins and an additional two upregulated proteins (Table S1). We conclude that IAA injection can achieve not only rapid and profound, but also highly specific degradation of AID-tagged proteins *in vivo*.

To assess the kinetics of protein degradation and recovery over longer periods following single dose I.P. administration of IAA, we generated *Ncaph*$^{AID:Clover/+}$ *Rosa26*$^{Tir1/Tir1}$ animals, in which AID-tagged protein could be degraded while leaving a pool of untagged protein to support ongoing cell division. Protein levels began to recover within 6 hours post-injection before returning to baseline levels within 72 hours (Figure 6C). This shows that degradation of endogenous proteins via the AID system is reversible *in vivo.*

Target protein was also efficiently degraded in 2 hours within mitotic crypt cells of the small intestine (Figure S5A). However we observed individual interphase cells that appeared resistant to degradation (Figure S5A, white arrow). Similarly, bone marrow erythroblasts (Ter119^{+}) retained Clover fluorescence after IAA exposure *in vivo* (Figure S5B). The barrier to degradation in this cell type was cell intrinsic rather than a property of the tissue environment, because Ter119^{+} cells in *ex vivo* bone marrow cultures also failed to degrade Ncaph in response to IAA treatment, whereas CD19^{+} cells in the same culture degraded efficiently (Figure S5C). Protein degradation was also inefficient in dividing spermatocytes (Figure

S5D). In this case, we speculate that the blood-testes barrier could prevent IAA from entering seminiferous tubules to effect protein degradation, although cell intrinsic barriers to degradation cannot be excluded.

Finally, we tested the ability of IAA to degrade AID:Clover-tagged Ncaph in embryos. Adult females homozygous for *Ncaph*$^{AID:Clover}$ and *Rosa26*^{Tir1} transgenes were mated with males of the same genotype, then injected I.P. with IAA (100 mg kg^{-1}) or vehicle at 10.5 days post coitum (Figure 6D). Embryos were collected 4 hours later, and Ncaph levels were quantified by immunofluorescence performed on whole mount embryonic cryosections co-stained with antibodies recognising E-Cadherin (Cdh1). This revealed near complete protein degradation within Cdh1 positive regions of the developing surface ectoderm (Figure 6E, 6F & 6G). These data show that IAA is able to cross the placenta to achieve robust protein degradation in embryonic cells.

Discussion

In this paper we describe a broadly applicable approach to study the consequences of acute protein loss in mammalian primary cells, tissues and whole organisms. The ability to trigger protein degradation using small molecules has numerous advantages over alternative reverse genetic approaches. Most importantly, protein function is removed in less than 2 hours; substantially quicker than would be possible using gene editing nucleases, recombinases or RNAi. Rapid removal is particularly important for studying essential cell cycle proteins such as condensins, where secondary and tertiary phenotypes arising downstream from abnormal cell division can quickly obscure primary phenotypes [31]. Given the central importance of condensins in establishing chromosome architecture during cell division [13,17,32,33], combined with persistent and unresolved questions about their involvement in other physiological processes in mammals [34-37], we anticipate that the two mouse models described here will provide an important resource for the chromosome biology community.

To demonstrate the utility of this system, we compared the ability of non-immortalised primary lymphocyte populations, from different lineages and stages of differentiation, to undergo a single round of cell division in the near absence of Ncaph and Ncaph2 (Figure 5). Our results show that different cell types differ in their ability to complete a single round of cell division in the near absence of these proteins, adding to an increasing body of data suggesting cell-type-specific differences in the consequences of condensin perturbation [38-41]. Elucidating the cause of these differences was beyond the scope of the current study, but it could potentially involve cell-type-specific chromosome topology (e.g. fewer catenations to remove in mature cells), or cell cycle checkpoints (e.g. greater sensitivity to mitotic arrest in precursor cells). In the future, we expect these two degrader mouse lines will provide valuable insights into chromosome biology and mitotic chromosome structure in the context of *in vivo* cellular heterogeneity, development and disease.

Protein degradation was achievable in a range of cell types, including B and T lymphocytes at different developmental stages (precursor and mature, Figure S3C), fibroblasts (Figure 2D), neural stem cells (Figure 2E), gut epithelial cells (Figure S5A), and embryonic Cdh1^{+} cells of the developing surface ectoderm (Figure 6G). However, a minority of cell types proved refractory. For example, erythroid progenitors failed to degrade AID-tagged proteins due to a cell intrinsic block (Figure

S5B & S5C). We speculate that erythroblasts lack one or more components of the ubiquitin proteosome system that is necessary for degradation via the AID system. Spermatocytes also failed to degrade (Figure S5D), likely due in part to poor ligand transit across the blood testes barrier. An analogous barrier prevents many small molecules from penetrating into the adult brain. Poor expression of condensins in post-mitotic tissues prevented us from testing AID function in the brain; however, a structurally related ligand for the AID2 system (5'Ph-IAA [16]) was found to have relatively weak protein degradation activity in this tissue.

By performing genetic crosses to generate animals with different allelic combinations we showed that the dosage of all three components of the ternary complex formed between the target protein, ligand and Tir1 substrate receptor protein, can determine the kinetics of protein degradation in mammalian primary cells (Figure 2E, Figure 3, Figure 4). This could have implications for understanding the activity of protein degrader drugs such as PROTACs and IMiDs. For example, variability in expression of the substrate receptor protein CRBN has been correlated with patient responses to iMID treatment in haematological malignancy [42]. Our data (Figure 3, Figure S2) provide empirical support for a causative link between substrate receptor dose and the protein degradation activity of molecular glue compounds. Moreover, our finding that high cellular doses of target protein reduce the overall efficiency of protein degradation (Figure 4) suggests that highly expressed proteins could, on average, make more challenging targets for chemical degradation strategies.

Concerns have been raised about the AID system because a subset of AID-tagged proteins can undergo Tir1-dependent turnover even in the absence of exogenous IAA. We showed that the presence of Tir1 had little or no effect on the expression of two different AID-tagged condensin subunit proteins in the absence of ligand (Figure 1G), but enabled their rapid degradation, often to levels below 10% of baseline, within 1 to 2 hours of ligand exposure (Figure 2, Figure 6). Regulated induction of Tir1 expression in yeast has demonstrated that leaky degradation of target proteins occurs as a consequence of Tir1 overexpression [28]. Achieving Tir1 expression levels sufficient for IAA-inducible degradation yet insufficient for IAA-independent degradation is therefore of paramount importance. That leaky degradation did not cause problems in our study suggests that the single-copy *Rosa26*^{Tir1} allele generated via genome editing is expressed within this desirable

range, at least for these two proteins. If leaky degradation were a problem for other target proteins, this could be kept to a minimum through the use of *Rosa26*^{Tir1} heterozygotes. While our work was ongoing, point mutations in Tir1 have been identified that, in combination with a modified ligand, eliminate Tir1-dependent leaky degradation, and allow degradation to be induced at much lower ligand concentrations [16]. We therefore predict that AID tagging should be applicable to study a broad range of intracellular proteins in mice and their primary cell derivatives.

A very recent preprint has reported targeted degradation of endogenously tagged NELFB protein using dTAG [43]: another promising degron-tagging approach [8,9]. dTAG uses distinct tags, ligands and E3 ligase interactions, and should therefore be compatible with the AID system developed here to enable orthogonal chemical control of two different proteins in mice. In contrast to AID, which requires exogenous expression of the E3 ligase protein Tir1, dTAG uses endogenous E3 ligases to achieve protein degradation and could therefore be simpler to establish in mice. However, this same property could also prevent future applications that require tissue- or cell-type selective protein degradation. This is achievable using AID via tissue-specific expression of Tir1, as shown in *C. elegans* [44,45]. Further work is needed to assess the safety and efficacy of each approach for protein degradation across targets, tissues, disease states and timescales. Nonetheless, our demonstration that degron tagging systems are effective in living mice should enable more versatile conditional alleles to study protein function, and to model drug activity, in mouse models of development and disease.

Materials and Methods:

Mouse maintenance and husbandry

All animal work was approved by a University of Edinburgh internal ethics committee and was performed in accordance with institutional guidelines under license by the UK Home Office. AID knock-in alleles were generated under project license PPL 60/4424. Rosa26^{Tir1} knockin mouse lines were generated under the Canadian Council on Animal Care Guidelines for Use of Animals in Research and Laboratory Animal Care under protocols approved by the Centre for Phenogenomics Animal Care Committee (20-0026H). Experiments involving double transgenic animals were conducted under the authority of UK project license PPL P16EFF7EE

Mice were maintained at the Biological Research Facility, Western General Hospital, Edinburgh. All experimental animals were between 6 and 16 weeks in age unless otherwise specified. Mice were housed in individually ventilated cages with 12 hour light/dark cycles. All tissues were harvested and processed immediately following euthanasia via cervical dislocation or CO_2.

Generation of Ncaph and Ncaph2 degron-reporter mice.

Ncaph-AID-mClover and *Ncaph2-AID-mClover* mice were generated following the Easi-CRISPR protocol [21]. sgRNAs were designed using the Zhang Lab design tool (crispr.mit.edu) and ordered from IDT. Priority was given to protospacer sequences that would result in cleavage proximal to the stop codon with low predicted likelihood for off-target cleavage. Repair templates were long single stranded oligonucleotides ('megamers') ordered from IDT. Each megamer comprised 105 nucleotides of homology either side of the integrated sequence. Integrations included linker sequence and the 44 amino acid mini auxin-inducible degron used by Nora et al [6,7] fused in-frame with the fluorescent protein Clover [46]. Full nucleotide sequences for the guide RNA target sequence and repair templates are listed in Appendix S1.

The microinjection mix comprised pre-annealed crRNA/TracrRNA complex (20ng/µl), repair template (5ng/µl), and Cas9 protein (NEB - 0.3 µM). This was incubated at 37°C for 10 minutes before microinjection. Zygotes were collected from C57BL/6J females mated overnight with C57BL6/J stud males (Charles River Laboratories). Editing reagents were introduced via intracytoplasmic microinjection at the Evans Transgenic Facility (University of Edinburgh), cultured to the blastocyst stage before transfer to pseudopregnant CD1 females. Successful integrations were identified by

PCR using primers spanning the integration sites, then confirmed by observing band shifts on western blots probed with antibodies against wildtype NCAPH and NCAPH2 (Figure 1C). Founder animals were outcrossed for two generations with C57BL6/J animals and then N2 siblings were intercrossed to obtain homozygotes.

Generation of Rosa26^{Tir1} knockin mice.

The plasmid donor for generating *Rosa26^{Tir1}* knockin mice was constructed as follows. A TIR1-9myc cassette was PCR amplified from the pBABE-TIR1-9myc plasmid (addgene 648945, a kind gift from Don Cleveland [47]). The cassette was inserted into MluI restriction site of the pR26 CAG AsiSI/MluI plasmid (addgene 74286, a kind gift from Ralf Kuehn [48]) by infusion cloning (Takara). The coding sequence of TIR1-9myc was separated from the CAG promoter by a loxp-STOP-loxp (LSL) cassette.

The Rosa26-LSL-osTIR1-9myc(CD1-Gt(ROSA)26Sor$^{em1(CAG-LSL-osTIR1-myc)Jrt}$) mouse line was generated using the 2C-HR-CRISPR method [15]. Cas9 mRNA (100ng/ul), R26 sgRNA (50ng/ul) and the Rosa26-LSL-osTIR1-9myc circular donor plasmid (30ng/ul) were microinjected into 2-cell stage embryos of CD1 mice. Full nucleotide sequences for the guide RNA target sequences and repair templates are listed in Appendix S1. Embryos were cultured overnight in KSOMaa (Cytospring) to reach the morula stage and then transferred to pseudopregnant CD1 females. 15 live pups were produced, 3 of them were validated to contain the correct insert by long range PCR. One male founder was crossed with wild a wildtype CD1 female to generate N1 offsprings. The N1s were first screened by long range PCR. For the positives, knock-in junction sequences were validated by sanger sequencing. Droplet Digital Quantitative PCR(ddqPCR) was performed by the The Center for Applied Genomics (TCAG) in Toronto to measure the copy number of the insert. All N1 animals tested had single copy insertions. The mouse line was outcrossed for another three generations to remove any possible off-target mutations that might have been induced by genome editing. The Rosa26-LSL-osTIR1-9myc mouse line is homozygous viable and were kept as homozygous breeding.

To generate the *Rosa26^{Tir1}* allele (full name *Rosa26-osTIR1-9myc (CD1-Gt(ROSA)$^{26Sorem1.1(CAG-LSL-osTIR1-myc)Jrt}$*) used in subsequent experiments, a *Rosa26-LSL-osTIR1-9myc$^{+/-}$* male was mated with a *pCX-NLS-cre (ICR-Tg(CAG-cre)^{1Nagy}*

female. Progeny were screened for removal of the LSL cassette by PCR and the mice carrying correctly recombined sequences were bred to establish the line. The *Rosa26*^{Tir1} allele is homozygous viable and mice were bred in the homozygous state.

Whole Cell Protein Extract Preparation & Quantification

Protein preparations were generated from either single cell suspensions of primary haematopoietic cells, or whole tissue. Single cell suspensions of thymus were generated by gentle dissociation of whole thymus tissue through 40 µm filters (Fisherbrand, 22-363-547). For bone marrow, tissue was flushed out of tibia and femur bones with PBS before dissociation through a 40 µm filter. Cell numbers were counted manually using a haemocytometer. Bone marrow cells were further purified by Magnetic Activated Cell Sorting (Miltenyi), using beads pre-coated with antibodies against B220, Ter-119, CD4 or CD8. MACS purification proceeded according to the manufacturers instructions. Cell pellets were resuspended in NP-40 Lysis Buffer (150mM NaCl, 50mM Tris-HCl, 1% NP-40**)** using 3 volumes of NP-40 Buffer to 1 volume of cell pellet. 0.5 µL benzonase nuclease (Millipore) was added per 100 µL of resuspended pellet. Samples were incubated at 4 °C for 30 minutes with intermittent vortexing, before pelleting cellular debris via centrifugation at maximum speed (13,200 g, 15 minutes, 4 °C). For whole tissue samples, adult tissue (brain, thymus, lung, spleen, kidney, small intestine and liver) were removed, snap frozen in LN2, and stored at -80°C until use. Between 10-30mg of frozen tissue was weighed and homogenised in 1mL RIPA buffer (150mM NaCl, 1%NP-40, 0.5% NaDeoxycholate, 0.1% SDS, 50mM Tris-HCl pH8 with 5µl benzonase (Millipore)) for 10 minutes using a TissueLyserLT (Qiagen), then incubated on ice for 30 minutes. Cellular debris was pelleted via centrifugation at maximum speed for 15 minutes at 4°C. Supernatants were transferred into fresh tubes, and protein concentration was quantified using a Pierce BCA Protein Assay Kit (Thermo, 23228) following manufacturer's instructions. Pierce Lane Marker Reducing Sample Buffer (1X, Thermo, 39000) was added to each sample prior to denaturation via boiling at 95 °C for 5 minutes. Samples were used immediately or stored at -20 °C.

Western Blotting

Denatured protein lysates (12.5 µg/sample) were loaded on to NuPAGE 4-12% Bis-Tris 1.0 mm Mini Protein Gels (Invitrogen, NP0321) alongside Chameleon Duo

Protein Ladder (3 µL/lane; LiCOR, 928-60000) or PageRuler Protein Ladder (5 µL/lane; Thermo Scientific, 26616) and run in pre-chilled 1X MOPS Buffer (Thermo, NP0001). Samples were typically run at 100 Volts for 90 minutes. Transfers were performed using either the iBlot2 Gel Transfer device according to manufacturer's instructions or wet transfer. PVDF membranes were pre-soaked in 100 % methanol (Fisher, 10284580) and rinsed briefly in Transfer Buffer (25 mM Tris (AnalaR, 103156X), 200 mM glycine (Fisher, G-0800-60), 20% methanol, 0.02% SDS (IGMM Technical Services)). Genie Blotter transfer device (Idea Scientific) was assembled with the gel and PVDF membrane placed between two layers of cellulose filter paper (Whatman, 3030-917) inside the loading tray. Once the apparatus was prepared, Transfer Buffer was filled to the top of the Genie Blotter and transfer proceeded for 90 minutes at 12 volts.

Conditions for blocking and antibody staining were optimised individually for each probe. Samples were blocked with either 5% milk powder (Marvel) in TBS (IGMM Technical Services) with 0.1% Tween20, or 3% BSA (Sigma) in TBS with 0.1% Tween20, with constant agitation, either at room temperature for 1 hour, or at 4 °C overnight.

Primary antibodies were added to the corresponding block solution at the dilution shown in Table S2. Membranes were incubated in the antibody dilutions with constant agitation, either at room temperature for 1 hour, or at 4 °C overnight. Membranes were washed in TBS-Tween20 solutions (0.1% Tween20; 4 washes x 10 minutes). Fluorescent or HRP-conjugated secondary antibodies were also diluted in the corresponding block solution (with 0.1% Tween20), and membranes were incubated with secondary antibody dilutions under constant agitation at room temperature for 1 hour. Membranes were then washed in TBS-Tween20 solutions (0.1% Tween20, 4 washes x 10 minutes). Membranes were visualised on an Odyssey CLx Imaging System (LiCOR) or ImageQuant (Cytiva). Fluorescent antibodies were detected using either a 700 Channel Laser Source (685 nm) or 800 Channel Laser Source (785 nm).

Proteome analysis by Mass Spectrometry

Mice were treated with 100mg/kg auxin via intraperitoneal injection for 2 hours, then culled by cervical dislocation. Thymus was removed and a single cell suspension of primary thymocytes was made using ice-cold PBS. $CD8a^+$ cells were isolated by

MACS using CD8a2 (Ly-2) microbeads (Miltenyi) following manufacturer instructions. Purified cells were lysed in whole proteome lysis buffer (6M GuHCl, 100mM TrisHCl 8.5, 1mg/mL Chloracetamide, 1.5mg/mL TCEP) at a concentration of $0.3x10^6$ cells/µL buffer. Lysate was sonicated with a probe sonicator (Soniprep 150) until no longer viscous, and boiled at 95°C for 5 minutes, then centrifuged at 14,000rpm for 5 minutes. Supernatent was then transferred to a fresh tube and processed for Mass spectrometry.

A 50uL volume of sample was heated to 97°C for 5 minutes, then pre-digest (Lys-C, Fujifilm WakoPure Chemical Corporation) was added (1µL/sample) and samples incubated at 37°C for 3 hours. Samples were diluted 1/5 by addition of 200uL Mass Spec grade water, and 1ug trypsin (Fujifilm WakoPure Chemical Corporation) was added to each sample. Samples were incubated at 37°C with hard shaking overnight.

Samples were acidified with 1% TFA and centrifuged at 13,000 rpm, for 10 minutes at room temperature. Sample was applied to a double layer Empore C18 Extraction Disk (3M) prepared with methanol. Membrane was washed twice with 0.1% TFA and protein was eluted with elution buffer (50% ACN, 0.05% TFA), dried using a CentriVap Concentrator (Labconco) and resuspended in 15uL 0.1% TFA. Protein concentration was determined by absorption at 280nm on a Nanodrop 1000, then 2 µg of de-salted peptides were loaded onto a 50 cm emitter packed with 1.9 µm ReproSil-Pur 200 C18-AQ (Dr Maisch, Germany) using a RSLC-nano uHPLC systems connected to a Fusion Lumos mass spectrometer (both Thermo, UK). Peptides were separated by a 140 min linear gradient from 5% to 30% acetonitrile, 0.5% acetic acid. The mass spectrometer was operated in DIA mode, acquiring a MS 350-1650 Da at 120k resolution followed by MS/MS on 45 windows with 0.5 Da overlap (200-2000 Da) at 30k with a NCE setting of 27. Raw files were analysed and quantified using Spectronaut 15 (Biognosis, Switzerland) using directDIA against the Uniprot Mus Musculus database with the default settings. Ratios and statistical tests were determined by the Spectronaut pipeline using default settings.

Flow Cytometry

For cultured adherent cells, single cell suspensions were first generated using trypsin (MEFs) or accutase (Neural Stem Cells). For haematopoietic cells, samples were prepared from single-cell suspensions of bone marrow and thymus. Samples

were incubated with fluorescently-conjugated antibodies against cell surface markers (Table S2) and Fixable Viability Dye (eBioscience, 65-0865-14, 1 in 200 dilution) diluted in Flow Cytometry Staining Buffer (eBioscience, 00-4222-26) (20 minutes at 4 °C). Samples were then washed in a 10-fold volume of Flow Cytometry Staining Buffer before centrifugation at 300 g for 5 minutes at 4°C. Pellets were resuspended in Cytofix/Cytoperm solution (BD Bioscience, 554722) following manufacturer's instructions and washed in Perm/Wash buffer (BD Bioscience, 554723). If required, samples were incubated with fluorescently conjugated antibodies against intracellular markers for 20 minutes at room temperature. For intracellular γH2AX staining, samples were further permeabilised by resuspending in Perm/Wash buffer (1 mL) for 15 minutes at 4 °C before antibody incubation. After intracellular antibody incubation, all stained samples were then washed in Perm/Wash buffer (300 g/ 5 minutes/ 4 °C). Cell Trace Yellow (Thermo Fisher C34567) experiments were conducted according to the manufacturer's protocol. Samples were resuspended in DAPI staining solution (1 µg/mL DAPI in PBS). DAPI-stained samples were incubated on ice for at least 15 minutes before data acquisition.

Data acquisition (BD LSRFortessa) was performed no more than 24 hours following sample preparation. Identical laser power was used to quantify Clover signal across all experiments. Data analysis was conducted using FlowJo software (Treestar). Cellular debris/aggregates were excluded using strict forward- and side-scatter gating strategies. Cell cycle stages were gated based on DNA content (DAPI) fluorescence. Wild-type samples lacking Clover expression were processed and stained in parallel to transgenic samples. To correct for autofluorescence, background fluorescence was measured for each cell population from wild-type samples, and then subtracted from transgenic fluorescence values. To generate boxplots, the background-corrected fluorescence value from each of >1000 cells was expressed relative to the mean of the vehicle only condition. We focused exclusively on S/G2/M cells, gated on DNA content, for quantifications to avoid the confounding effects of quiescent cells, where condensins are expressed at very low levels.

Primary cell culture:

Thymic & Bone Marrow *ex vivo* cultures:

Single cell suspensions of thymus tissue were generated by gentle dissociation of whole thymus tissue through 40 µm filters (Fisherbrand, 22-363-547) into PBS. For bone marrow, tissue was flushed out of tibia and femur bones with PBS before dissociation through a 40 µm filter. Cell numbers were counted manually using a haemocytometer. Cells (1-2.5 x10^6/mL) were then cultured at 37 °C *ex vivo* for 2-6 hours in RPMI (Gibco, 21875-034) containing 10% FCS (IGC Technical Services) and penicillin (70 mg/L, IGC Technical Services) and streptomycin (130 mg/L, IGC Technical Services). For bone marrow cultures, different cell lineages were cultured together and then B cell and erythroid lineages were identified based on flow cytometric detection of cell surface marker expression (CD19 and Ter119, respectively) and analysed separately.

Peripheral T and B lymphocyte *ex vivo* cultures

Peripheral T and B lymphocytes were derived from spleens dissected from adult animals. Single cell suspensions of splenic tissue were generated by gentle dissociation of whole spleen through 40 µm filters (Fisherbrand, 22-363-547). Splenic cells were resuspended in MACS buffer (0.5% BSA (Sigma), 1 mM EDTA in PBS – 40 µL MACS Buffer per 10 x 10^7 cells) in preparation for Magnetic Activated Cell Sorting. Peripheral T- and B-cells were isolated from whole spleen using Pan T Cell (Miltenyi Biotec,130-095-130) or Pan B Cell (Miltenyi Biotec, 130-104-433) isolation kits, respectively, according to the manufacturer's instructions.

Isolated peripheral T- and B-cells were cultured at a density of 0.5 x10^6 cells/mL, in RPMI media (Gibco, 21875-034) supplemented with 10% FCS (IGC Technical Services), penicillin (70 mg/L, IGC Technical Services), streptomycin (130 mg/L, IGC Technical Services), 2 mM L-Glutamine (IGC Technical Services), 1mM sodium pyruvate (Sigma-Aldrich, S8363), 50 µM β-mercaptoethanol (Gibco, 31350-010) and 1x Non Essential Amino Acids (Sigma-Aldrich, M7145) at 37 °C. To stimulate cells, T-cells were additionally cultured with 30 U/mL IL-2 (Peprotech, 212-12) and 1 µL/mL Mouse T-Activator Dynabeads (Gibco, 11452D), whilst B-cells were cultured with 10 ng/mL IL-4 (Peprotech, 214-14) and 5 µg/mL LPS (Sigma, L4391). Cells were allowed to proliferate for 48 hours prior to any auxin/BrdU treatments.

MEFs

MEFs were derived from E13.5/E14.5 embryos. Head and organs were removed, and the embryonic body was homogenized with a sterile razor blade. 1 mL 1X Trypsin (Sigma-Aldrich, T4174) in PBS was added per 3 embryos and the mixture was incubated at 37 ^{o}C for 10 minutes. Tissue was further homogenized by passage through a 23G needle approximately 20 times. Homogenous tissue was then resuspended in MEF media (Standard DMEM (Gibco, 41965-039) with 15% FCS (IGC Technical Services), penicillin (70 mg/L) and streptomycin (65 mg/L), 2 mM L-Glutamine (IGC Technical Services), 1mM sodium pyruvate (Sigma-Aldrich, S8363), 50 µM β-mercaptoethanol (Gibco, 31350-010), 1x Non Essential Amino Acids (Sigma-Aldrich, M7145)) and passed through a 40 µm filter to remove non-homogenised tissue. MEFs were then cultured in a T75 flask (per 3 embryos) at 37 ^{o}C, 5% CO_2, and 3% O_2.

Neural Stem Cells

SC lines were derived from the telencephalon of individual E13.5 or E15.5 embryos following a previously described protocol [49].
Once stably propagating, NSCs were cultured in T75 flasks. When passaging, NSCs were washed with Wash Media (WM) (DMEM/Ham's F-12 media with l-Glutamine (Sigma-Aldrich, D8437-500), 300 mM D-(+)-Glucose solution (Sigma-Aldrich, G8644), 1X MEM Non-Essential Amino Acids Solution (Gibco, 11140050), 4.5 mM HEPES (Gibco, 15630056), 75 mg/mL BSA solution, 50 µM β-mercaptoethanol (Gibco, 31350-010), penicillin (70 mg/L, IGC Technical Services) and streptomycin (130 mg/L, IGC Technical Services)) and propagated in Complete Media (CM) (WM supplemented with Epidermal Growth Factor (EGF) (PeproTech, 315-09) and Recombinant Human FGF-basic (FGF) (PeproTech, 100-18B) each to final concentration of 10 ng/ml, 1 µg/mL Laminin (Trevigen, 3446-005-01), 2.5 mL N-2 Supplement (100X) (Gibco, 17502048) and 5 mL B27 Supplement (50X) (Gibco, 17504044)). Cells were cultured at 37 ^{o}C, 5% CO2 and passaged every 2-3 days.

Auxin treatment

Cell Culture

Indole-3-acetic acid (auxin, MP Biomedicals, 102037) was solubilised in DMSO to give a 500 mM stock solution. This stock solution was then diluted in the cell media of choice to give a solution of desired concentration before being filter-sterilised through a 0.22 µm filter (Starlab, E4780-1226). A DMSO-only treated sample was always processed alongside any auxin treated sample.

in vivo

Indole-3-acetic acid powder (125 mg) was dissolved in 1 mL PBS (Sigma-Aldrich, D8537), with small quantities of NaOH (IGC Technical Services, 5 M, 140 µL) added to help solubilise the drug. The solubilised drug was then added to 2.4 mL PBS, with minute volumes of HCl (5 M, Fisher, H/1150/PB17) added until solution pH reached 7.4. In order to achieve a more physiological osmolarity, the drug mixture was diluted to 10 mL in MQ water (final osmolarity range of ~355 - 380 mOsm/L; concentration = 71.4 mM). Vehicle injection mixture was prepared by adding 10 µL of both NaOH (5M) and HCl (5M) to 10 mL PBS (final osmolarity of 326 mOsm/L).

Both vehicle and auxin injection mixtures were filter-sterilised through 0.22 µm filters prior to injection. Sterile auxin solution was then administered to animals via intraperitoneal injection. Auxin injection volume was adjusted based on animal weight so that each animal received 100 mg of auxin per kg of body weight. Animals were culled using a schedule 1 approved method at appropriate timepoints, and tissues of interest were dissected and stored briefly on ice until further processing.

BrdU Pulse Chase Assay

A 10 mM stock of BrdU was firstly generated by dissolving 0.0031 g BrdU powder (Sigma-Aldrich, B5002) in 1 mL PBS. Samples were firstly pre-depleted of Ncaph/Ncaph2 using auxin (500 µM) for 2-3 hours, before being pulsed with BrdU (final concentration = 10 µM) for 30 minutes at 37 ^{o}C. BrdU was washed out by firstly pelleting cells via centrifugation (300 g, 5 minutes) before washing once in media, and then pelleting samples again. Samples were then split in two, with half of the sample placed on ice for assessment of degradation efficiency at the beginning of the chase (0h time-point in Figure S3C). The other half of the sample was resuspended in pre-warmed auxin-containing media before being incubated at 37 ^{o}C for a further 3.5 hours. All samples were rinsed in PBS and pelleted after their

incubations were complete and stained with Fixable Viability Dye (eBioscience, 65-0865-14, 1 in 200 dilution), and/or fluorescent surface markers if required (20 minutes/ 4 °C), before being washed in 2 mL FCSB. To quantify the efficiency of auxin-induced depletion (Figure S3C), a small portion of each sample was taken at the start (0h) and end (3.5h) of the chase and analysed on the LSRFortessa. Degradation was calculated as described in the 'Flow Cytometry' section. Following the chase, the majority of each sample was then resuspended and fixed in Cytofix/Cytoperm solution (100 µL/sample, BD Bioscience, 554722) following manufacturer's instructions and washed in Perm/Wash buffer (2 mL/sample, BD Bioscience, 554723) before being resuspended in 0.5 mL FCSB and left overnight at 4 °C.

Samples were pelleted and resuspended in Cytoperm Permeabilisation Buffer Plus (BD Bioscience, 561651) following manufacturer's instruction, before being washed in 2 mL Perm/Wash buffer. Cytofix/Cytoperm solution (100 µL/sample) was used to re-fix samples for 5 minutes at 4 °C before samples were again washed in 2 mL Perm/Wash buffer. DNase I solution (eBioscience, 00-4425-10 – part of BrdU Staining Kit for Flow Cytometry, 8817-6600-42) was diluted following manufacturer's instruction. Each sample was resuspended in 100 µL diluted DNase I and incubated at 37 °C for 1 hour to expose the BrdU epitope. Samples were washed in 2 mL Perm/Wash solution, before being incubated with AlexaFluor-647-conjugated anti-BrdU monoclonal antibody (Invitrogen, B35140, 1 in 20 dilution in Perm/Wash, 20 minute incubation at room temperature). Perm/Wash (2 mL per sample) was used to wash samples. To stain for DNA content, each sample was resuspended in 20 µL 7-AAD (BD Biosciences, 559925) for at least 15 minutes before samples were finally diluted in 0.5 mL PBS. Samples were all analysed on the LSRFortessa as above.

Immunofluorescence on tissue cryosections

Tissues were dissected immediately *post-mortem* then washed in ice cold PBS, fixed for 24 hours (small intestine) or 2 hours (E10.5 embryos) in 4% PFA in PBS, then passed through 10 and 30% sucrose in PBS solutions, and mounted in OCT (Tissue-Tek). 20µm sections were cut on a Leica CM1850 and adhered to Superfrost Plus slides (Epredia). Sections were post-fixed in 4% PFA in PBS for 10 minutes at room temperature, then permeablised in 0.5% Triton X-1000 for 5 minutes at room

temperature, and washed twice in 0.2% Triton X-1000 for 5 minutes at room temperature. Sections were then blocked in 4% BSA in PBS for 1 hour (small intestine) or 2 hours (E10.5 embryo) at room temperature, and primary antibodies were diluted in 4% BSA in PBS and applied overnight at 4C. Sections were washed three times in 0.2% Triton X-1000, and secondary antibodies were diluted in 4% BSA in PBS and applied at room temperature for 2 hours. Sections were then washed as previously, stained with DAPI at 1µg/mL, and mounted in Vectashield (Vector Labs). To reduce autofluorescence, staining of small intestine sections also included an additional treatment with 0.1% Sudan Black in 70% ethanol at room temperature for 20 minutes immediately prior to DAPI stain and mounting.

Image Capture and Analysis

Images of small intestine sections were acquired at 100X magnification using a Photometrics Coolsnap HQ2 CCD camera and a Zeiss AxioImager A1 fluorescence microscope with a Plan Apochromat 100x 1.4NA objective, a Nikon Intensilight Mercury based light source (Nikon UK Ltd, Kingston-on-Thames, UK) and either Chroma #89014ET (3 colour) or #89000ET (4 colour) single excitation and emission filters (Chroma Technology Corp., Rockingham, VT) with the excitation and emission filters installed in Prior motorised filter wheels. A piezoelectrically driven objective mount (PIFOC model P-721, Physik Instrumente GmbH & Co, Karlsruhe) was used to control movement in the z dimension. Hardware control and image capture were performed using Nikon Nis-Elements software (Nikon UK Ltd, Kingston-on-Thames, UK). Deconvolution of 3D data was performed in Nis-Elements (Richardson Lucy, 20 iterations). 3D datasets were visualised and analysed for fluorescence intensity using Imaris V9.5 (Bitplane, Oxford Instruments, UK). DNA volume was calculated by manually rendering a surface around the DAPI signal in pH3S10^{+} cells within Imaris, and immunofluorescence signal was calculated from mean voxel intensity within that surface. The percentage protein remaining following IAA treatment was calculated by setting the mean voxel intensity measured in pH3S10^{+} cells from negative control (e.g. *Ncaph*$^{+/+}$ *Ncaph2*$^{+/+}$) sections to 0%, and the mean voxel intensity from vehicle-treated sections to 100%.

Images of embryonic whole-mount cryosections were acquired in 2D using a Zeiss Axioscan Z1 with a Plan-Apochomat 40x 0.95Korr M27 objective and an Axiocam 506 camera using DAPI channel as focus. Images were acquired in Zen 3.1

790 software, and analysed using QuPath 0.3.0 [50]. 5 regions per embryo were selected
791 based on lineage marker staining (Cdh1, Pdgfr), and mean pixel intensity was
792 calculated in the 647 channel, corresponding to Ncaph-AID:Clover detected with an
793 anti-GFP-647 nanobooster. The percentage protein remaining value was then
794 calculated as described for small intestine sections.
795
796 **Acknowledgements**
797 We thank the University of Edinburgh Transgenic Facility for performing CRISPR
798 microinjections to generate AID:Clover-tagged mouse lines, the Biological Research
799 Facility at the Western General Hospital for animal husbandry, the IGC Flow
800 Cytometry Facility, IGC Advanced Imaging Resource and IGC Mass Spectrometry
801 facility for technical support. We acknowledge technical support from the Model
802 Production Core staff led by M. Gertsenstein at the Centre for Phenogenomics for
803 generating the TIR1 knock-in mouse lines and Eszter Posfai (Princeton University)
804 for early collaboration efforts the proof of principle studies of AID in mouse embryos;
805 We are grateful to Luke Boulter for antibodies and advice on whole mount
806 immunofluorescence, and to Wendy Bickmore for comments on the manuscript. We
807 also acknowledge Masato Kanemaki and co-workers for their pioneering efforts to
808 develop the auxin-inducible degron system. Requests for the Rosa26^{Tir1} transgenic
809 mouse line should be addressed to Bin Gu (guibin1@msu.edu), and requests for the
810 Ncaph- and Ncaph2-AID:Clover lines should be addressed to Andrew Wood
811 (Andrew.j.wood@ed.ac.uk). This work was supported by a Sir Henry Dale Fellowship
812 from the Wellcome Trust (AW 102560/Z/13/Z), an MRC Unit award to the MRC
813 Human Genetics Unit, and Funding from CIHR (JR FDN-143334).
814
815 **Author contributions**
816 **L.M.** Led the development and validation of the two AID:Clover alleles, the primary
817 cell work in Figures 1 – 5, S1, S2 and S3 of the manuscript, and supported GT in
818 work shown in Figure 6, S4 and S5.
819 **G.T.** Led the *in vivo* work in Figures 6, S4 and S5, of the manuscript, supported L.M.
820 in developing the two AID:Clover alleles and in work for Figures 1 and 2 and S1.

J.B. Performed the Neural Stem Cell experiments in Figure 2 and the Cell Trace experiments in Figure S3.

E.C. Performed the whole mount immunofluorescence experiments in Figure 6, supervised by G.T.

L.S. performed immunofluorescence on MEFs shown in Figure 1.

A.K. captured and analysed the mass spectrometry data using samples provided by G.T.

J.R. conceived the study to develop TIR1 knock-in mouse lines; Provided supervision and funding for generating the Tir1 lines.

B.G. conceived the study to develop TIR1 knock-in mouse lines; designed and generated the TIR1 knock-in mouse lines.

A.W. conceived and designed the Ncaph- and Ncaph2-knockin lines, conceived, supervised and provided funding for all of the experimental work in the paper other than developing the TIR1 knockin mouse line, and wrote the paper with input from B.G, J.R, L.M and G.T.

Competing Financial Interest

The authors declare no competing financial interests.

840 References

841 1. Kos, C. H. Cre/loxP system for generating tissue-specific knockout mouse
842 models. *Nutr Rev* **62,** 243–246 (2004).
843 2. Nishimura, K., Fukagawa, T., Takisawa, H., Kakimoto, T. & Kanemaki, M. An
844 auxin-based degron system for the rapid depletion of proteins in nonplant cells.
845 *Nat Meth* **6,** 917–922 (2009).
846 3. Natsume, T. & Kanemaki, M. T. Conditional Degrons for Controlling Protein
847 Expression at the Protein Level. *Annu. Rev. Genet.* **51,** 83–102 (2017).
848 4. Tan, X. *et al.* Mechanism of auxin perception by the TIR1 ubiquitin ligase.
849 *Nature* **446,** 640–645 (2007).
850 5. Natsume, T., Kiyomitsu, T., Saga, Y. & Kanemaki, M. T. Rapid Protein
851 Depletion in Human Cells by Auxin-Inducible Degron Tagging with Short
852 Homology Donors. *Cell Reports* **15,** 210–218 (2016).
853 6. Nora, E. P. *et al.* Targeted Degradation of CTCF Decouples Local Insulation of
854 Chromosome Domains from Genomic Compartmentalization. *Cell* **169,** 930–
855 944.e22 (2017).
856 7. Morawska, M. & Ulrich, H. D. An expanded tool kit for the auxin-inducible
857 degron system in budding yeast. *Yeast* **30,** 341–351 (2013).
858 8. Nabet, B. *et al.* The dTAG system for immediate and target-specific protein
859 degradation. *Nat. Chem. Biol.* **14,** 431–441 (2018).
860 9. Nabet, B. *et al.* Rapid and direct control of target protein levels with VHL-
861 recruiting dTAG molecules. *Nat Comms* **11,** 4687–8 (2020).
862 10. Buckley, D. L. *et al.* HaloPROTACS: Use of Small Molecule PROTACs to
863 Induce Degradation of HaloTag Fusion Proteins. *ACS Chem Biol* **10,** 1831–
864 1837 (2015).
865 11. Boija, A. *et al.* Transcription Factors Activate Genes through the Phase-
866 Separation Capacity of Their Activation Domains. *Cell* **175,** 1842–1855.e16
867 (2018).
868 12. Narita, T. *et al.* Enhancers are activated by p300/CBP activity-dependent PIC
869 assembly, RNAPII recruitment, and pause release. *Molecular Cell* **81,** 2166–
870 2182.e6 (2021).
871 13. Gibcus, J. H. *et al.* A pathway for mitotic chromosome formation. *Science* **359,**
872 eaao6135 (2018).
873 14. Hégarat, N. *et al.* Cyclin A triggers Mitosis either via the Greatwall kinase
874 pathway or Cyclin B. *The EMBO Journal* **39,** e104419 (2020).
875 15. Gu, B., Posfai, E. & Rossant, J. Efficient generation of targeted large insertions
876 by microinjection into two-cell-stage mouse embryos. *Nat Biotechnol* **36,** 632–
877 637 (2018).
878 16. Yesbolatova, A. *et al.* The auxin-inducible degron 2 technology provides sharp
879 degradation control in yeast, mammalian cells, and mice. *Nat Comms* **11,**
880 5701–13 (2020).
881 17. Ono, T. *et al.* Differential Contributions of Condensin I and Condensin II to
882 Mitotic Chromosome Architecture in Vertebrate Cells. *Cell* **115,** 109–121
883 (2003).
884 18. Terakawa, T. *et al.* The condensin complex is a mechanochemical motor that
885 translocates along DNA. *Science* (2017). doi:10.1126/science.aan6516
886 19. Takagi, M. *et al.* Ki-67 and condensins support the integrity of mitotic
887 chromosomes through distinct mechanisms. *Journal of Cell Science* **131,**
888 jcs212092 (2018).
889 20. Samejima, K. *et al.* Functional analysis after rapid degradation of condensins

and 3D-EM reveals chromatin volume is uncoupled from chromosome architecture in mitosis. *Journal of Cell Science* **131,** jcs210187 (2018).

21. Miura, H., Quadros, R. M., Gurumurthy, C. B. & Ohtsuka, M. Easi-CRISPR for creating knock-in and conditional knockout mouse models using long ssDNA donors. *Nat Protoc* **13,** 195–215 (2018).
22. Quadros, R. M. *et al.* Easi-CRISPR: a robust method for one-step generation of mice carrying conditional and insertion alleles using long ssDNA donors and CRISPR ribonucleoproteins. *Genome Biol.* **18,** 92–15 (2017).
23. Nishide, K. & Hirano, T. Overlapping and Non-overlapping Functions of Condensins I and II in Neural Stem Cell Divisions. *PLoS Genet* **10,** e1004847 (2014).
24. Houlard, M. *et al.* Condensin confers the longitudinal rigidity of chromosomes. *Nat Cell Biol* **17,** 771–781 (2015).
25. Walther, N. *et al.* A quantitative map of human Condensins provides new insights into mitotic chromosome architecture. *The Journal of Cell Biology* jcb.201801048 (2018). doi:10.1083/jcb.201801048
26. Gu, B., Posfai, E., Gertsenstein, M. & Rossant, J. Efficient Generation of Large-Fragment Knock-In Mouse Models Using 2-Cell (2C)-Homologous Recombination (HR)-CRISPR. *Curr Protoc Mouse Biol* **10,** e67 (2020).
27. Sathyan, K. M. *et al.* An improved auxin-inducible degron system preserves native protein levels and enables rapid and specific protein depletion. *Genes & Development* **33,** 1441–1455 (2019).
28. Mendoza-Ochoa, G. I. *et al.* A fast and tuneable auxin-inducible degron for depletion of target proteins in budding yeast. *Yeast* **36,** 75–81 (2019).
29. Smith, E. D. *et al.* More than blood, a Novel Gene Required for Mammalian Postimplantation Development. *Molecular and Cellular Biology* **24,** 1168–1173 (2004).
30. Kreslavsky, T. *et al.* β-Selection-Induced Proliferation Is Required for αβ T Cell Differentiation. *Immunity* **37,** 840–853 (2012).
31. Hocquet, C. *et al.* Condensin controls cellular RNA levels through the accurate segregation of chromosomes instead of directly regulating transcription. *eLife* **7,** (2018).
32. Hirano, T., Kobayashi, R. & Hirano, M. Condensins, chromosome condensation protein complexes containing XCAP-C, XCAP-E and a Xenopus homolog of the Drosophila Barren protein. *Cell* **89,** 511–521 (1997).
33. Ganji, M. *et al.* Real-time imaging of DNA loop extrusion by condensin. *Science* eaar7831 (2018). doi:10.1126/science.aar7831
34. Rawlings, J. S., Gatzka, M., Thomas, P. G. & Ihle, J. N. Chromatin condensation via the condensin II complex is required for peripheral T-cell quiescence. *The EMBO Journal* **30,** 263–276 (2010).
35. Swygert, S. G. *et al.* Condensin-Dependent Chromatin Compaction Represses Transcription Globally during Quiescence. *Molecular Cell* (2018). doi:10.1016/j.molcel.2018.11.020
36. Dowen, J. M. *et al.* Multiple structural maintenance of chromosome complexes at transcriptional regulatory elements. *Stem Cell Reports* **1,** 371–378 (2013).
37. Wu, S. *et al.* ARID1A spatially partitions interphase chromosomes. *Sci Adv* **5,** eaaw5294 (2019).
38. Gosling, K. M. *et al.* A mutation in a chromosome condensin II subunit, kleisin β, specifically disrupts T cell development. *Proceedings of the National Academy of Sciences* **104,** 12445–12450 (2007).

39. Woodward, J. *et al.* Condensin II mutation causes T-cell lymphoma through tissue-specific genome instability. *Genes & Development* **30,** 2173–2186 (2016).
40. Martin, C.-A. *et al.* Mutations in genes encoding condensin complex proteins cause microcephaly through decatenation failure at mitosis. *Genes & Development* **30,** 2158–2172 (2016).
41. Elbatsh, A. M. O. *et al.* Distinct Roles for Condensin's Two ATPase Sites in Chromosome Condensation. *Molecular Cell* **76,** 724–737.e5 (2019).
42. Heintel, D. *et al.* High expression of cereblon (CRBN) is associated with improved clinical response in patients with multiple myeloma treated with lenalidomide and dexamethasone. *Br J Haematol* **161,** 695–700 (2013).
43. Abuhashem, A. & Hadjantonakis, A.-K. Rapid and efficient adaptation of the dTAG system in mammalian development reveals stage specific requirements of NELF. *bioRxiv* 2021.11.30.470581 (2021).
44. Ashley, G. E. *et al.* An expanded auxin-inducible degron toolkit for Caenorhabditis elegans. *Genetics* **217,** (2021).
45. Zhang, L., Ward, J. D., Cheng, Z. & Dernburg, A. F. The auxin-inducible degradation (AID) system enables versatile conditional protein depletion in C. elegans. *Development* **142,** 4374–4384 (2015).
46. Lam, A. J. *et al.* Improving FRET dynamic range with bright green and red fluorescent proteins. *Nat Meth* **9,** 1005–1012 (2012).
47. Holland, A. J., Fachinetti, D., Han, J. S. & Cleveland, D. W. Inducible, reversible system for the rapid and complete degradation of proteins in mammalian cells. *Proc. Natl. Acad. Sci. U.S.A.* **109,** E3350–7 (2012).
48. Chu, V. T. *et al.* Efficient generation of Rosa26 knock-in mice using CRISPR/Cas9 in C57BL/6 zygotes. *BMC Biotechnol.* **16,** 4 (2016).
49. Pollard, S. M. In vitro expansion of fetal neural progenitors as adherent cell lines. *Methods Mol. Biol.* **1059,** 13–24 (2013).
50. Bankhead, P. *et al.* QuPath: Open source software for digital pathology image analysis. *Sci. Rep.* **7,** 16878–7 (2017).

Figure Legends

Figure 1: Mouse models for auxin-inducible degradation of condensin proteins

A. Schematic diagrams showing the subunit composition of condensin I and II complexes with C-terminal AID:Clover. The kleisin subunits of condensin I and II are Ncaph and Ncaph2, respectively. **B.** CRISPR-Cas9 strategy for integrating mClover cassettes at the Ncaph and Ncaph2 loci using long single stranded deoxyoligonucleotides (ssODN) to generate *Ncaph*$^{AID:Clover}$ and *Ncaph2*$^{AID:Clover}$ alleles. Full details and sequences for the integrated cassettes are given in Appendix S1. **C**. Western blots prepared from thymic whole cell protein extract were probed with antibodies recognising endogenous Ncaph or Ncaph2, with tubulin as a loading control. '+' indicates wildtype allele, 'tag' indicates AID:Clover. **D.** Immunofluorescence imaging of mitotic murine embryonic fibroblast lines derived from *Ncaph*$^{AID:Clover/AID:Clover}$ and *Ncaph2*$^{AID:Clover/AID:Clover}$ embryos. Scale bar = 5 μm. **E.** Schematic diagram showing the Rosa26^{Tir1} allele. Details on how this allele was generated are in Figure S1D and the materials and methods. **F.** Breeding scheme to combine endogenously-tagged *Ncaph* and *Ncaph2* alleles with *Rosa26*^{Tir1}. **G.** Clover fluorescence was measured by flow cytometry in primary S/G2/M thymocytes (gated on DNA content, n > 1000 cells/sample) from mice homozygous for AID:Clover-tagged target proteins, in combination with 0, 1 or 2 alleles of the Rosa26^{Tir1} transgene. Cells were not subjected to IAA treatment. Boxplots show background-corrected mean fluorescence values from (n) biological replicate samples. * indicates a significant ($p<0.05$) difference between genotypes (one-way ANOVA with Tukey HSD test, $p < 0.05$). NS: not significant.

Figure S1: Supplement to Figure 1

A. Observed and expected genotype frequencies among 28 day-old animals generated from heterozygous crosses for each AID:Clover transgene (tag). Chi-squared tests revealed no significant deviation from expected mendelian frequencies. **B.** Litter sizes from matings between animals heterozygous versus homozygous for each AID:Clover transgene. * indicates significant difference at $p < 1 \times 10^{-3}$ from unpaired two-tailed t-tests **C.** Weight of pups at 28 days post-partum from crosses between parents heterozygous for the AID:Clover transgene (tag/+). M = male, F = female. * indicates significant differences between genotypes at $p < 0.01$, ** at $p < 0.05$ from one-way ANOVA with Tukey's HSD posthoc test. **D.** Schematic illustrating the derivation of Rosa26^{Tir1} via a Rosa26$^{LSL\text{-}Tir1}$ intermediate. Breeding of Rosa26$^{pCAG\text{-}LSL}$ mice to pCX-NLS-cre caused germline deletion of the lox-stop-lox cassette to produce Rosa26^{Tir1}. **E.** Western blots of whole tissue extracts from Rosa26$^{Tir1/Tlr1}$ or Rosa26$^{+/+}$ animals, probed with an anti-myc tag antibody (9B11). **F.** Observed and expected genotype frequencies among 28 day-old animals generated from crosses between parents homozygous for either *Ncaph*- or *Ncaph2*$^{AID:Clover}$ and heterozygous for *Rosa26*^{OsTir1}. Chi-squared tests revealed no significant deviation from expected mendelian frequencies of Rosa26 genotypes in the *Ncaph* background, and elevated frequencies of Rosa26^{Tir1} homozygotes in the *Ncaph2* background. **G.** Litter sizes from any mating involving a male (M) or female (F) carrying *Rosa26*^{Tir1} and either *Ncaph*- or *Ncaph2*$^{AID:Clover}$ alleles in the homozygous state, in combination with animals of various genotype. Because genotypes of the other animal in each mating differed between conditions, these data show simply that breeding from double homozygous transgenic mice is possible and are not suitable to quantify fertility across conditions. **H.** Weight of pups at 28 days post-partum. Differences between Tir1 genotypes were not significant at $p < 0.05$ in one-way ANOVA tests. M = male, F = female.

Figure 2: Rapid and titratable degradation of endogenous *Ncaph* and *Ncaph2* in primary cells

A. Schematic illustration of experiments designed to test targeted degradation of condensin subunits in primary cells. **B.** Western blots prepared from thymus whole cell extract and probed with polyclonal antibodies against Ncaph, Ncaph2, or a Gapdh loading control. Robust tag-dependent degradation of target proteins is clearly evident after 3 hours of auxin treatment. **C & D.** Boxplots quantify the extent of targeted protein depletion following IAA treatment (500μM for 3 hours), measured by flow cytometry in primary CD8^{+} thymocytes (C) and embryonic fibroblasts (D). n = 3 biological replicates from at least 2 independent

experiments, with degradation measured in over 1000 S/G2/M cells in each case. To calculate % protein remaining, the background corrected fluorescence value of each cell was expressed as a percentage of the mean fluorescence value for all cells in the vehicle-only condition. Boxes show the boundaries of upper and lower quartiles and whiskers show the range. Where negative values were observed (e.g. in MEFs due to variable autofluorescence between lines), a value of 0% was assigned. **E.** Titration of target protein levels in primary neural stem cells treated with different IAA concentrations for 2 hours. Boxplots were generated as described for panels C&D.

Figure 3: Tir1 dosage determines degradation kinetics of AID-tagged proteins.
A. Schematic diagram illustrates the assembly of the Tir1 substrate receptor protein, IAA ligand and AID tagged target protein-of-interest into a ternary complex necessary for target protein ubiquitination via SCF^{Tir1}, and degradation. **B & C**. Histograms show the distribution of Clover expression levels, measured by flow cytometry in S/G2/M thymocytes cultured for 2 hours *ex vivo* in the presence of different IAA concentrations. Thymocytes were isolated from animals homozygous for either (B) $Ncaph^{AID:Clover}$ or (C) $Ncaph2^{AID:Clover}$ alleles in combination with either one (dark purple) or two (light purple) alleles of $Rosa26^{Tir1}$. Equivalent data from animals heterozygous for AID-tagged alleles is shown in Figure S3. **D.** Comparison of depletion kinetics in the presence of one (black) versus two (red) alleles of the Tir1 transgene at low (solid line) versus high (dashed line) ligand concentrations (n = 3 biological replicate samples). Each experiment in panels B – D used data from at least 1000 S/G2/M thymocytes, gated on DNA content. In panel D, the mean background-corrected fluorescence value for each cell population is expressed as a percentage of the mean background-corrected fluorescence value for the vehicle only condition.

Figure S2: Supplement to Figure 3
Histograms show the distribution of Clover expression levels, measured by flow cytometry in >1000 S/G2/M thymocytes cultured for 2 hours *ex vivo* in the presence of different IAA concentrations. Thymocytes were isolated from animals heterozygous for either (**A**) $Ncaph^{AID:Clover}$ or (**B**) $Ncaph2^{AID:Clover}$ alleles in combination with either one (dark purple) or two (light purple) alleles of $Rosa26^{Tir1}$.

Figure 4: Dosage of AID-tagged proteins controls their degradation kinetics
A. The relative expression of Ncaph and Ncaph2 (n = 6 biological replicates each) in S/G2/M thymocytes, based on flow cytometric Clover fluorescence measurements in > 1000 cells. **B**. Table showing the relative total dose of AID tagged proteins in mice heterozygous for $Ncaph2^{AID:Clover}$ in combination with either 0 (Low), 1 (Medium) or 2 (High) alleles of $Ncaph^{AID:Clover}$. Relative AID dose is calculated based on data in panel A. **C.** Schematic showing the time course for auxin treatment of primary thymocytes in panels D&E. **D.** Western blots probed with a polyclonal antibody against Ncaph2. Tagged protein (upper band) is degraded, whereas wildtype protein (lower band) is not. * indicates non-specific band. **E**. Quantification of Ncaph2-AID:Clover depletion in the presence of low, medium or high overall AID-tagged protein dose. Density of the AID:Clover band (see panel D) was first measured relative to the corresponding wildtype allele (bottom) as an internal control. The AID:WT ratio in the vehicle only control was set at 100% and IAA treatment conditions were then calculated relative to this value. Data from two independent experiments are presented.

Figure 5: Dynamic changes in condensin dependency during lymphocyte differentiation
A. Chronological representation of the BrdU pulse chase assay to measure the efficiency of cell division in primary cell types cultured *ex vivo*. Lymphocyte isolation and culture protocols are detailed in the materials and methods. Quantifying the % of $BrdU^+$ cells (**B**) that complete mitosis and halve their DNA content (**C**) allows the efficiency of a single cell division to be quantified under normal or acute condensin deficient conditions. The appearance of $BrdU^+G1$ cells can be seen at 3 and 5 hours. **D.** Representative DNA content

profiles, gated on BrdU$^+$ as shown in panel B, from cycling early (thymic / marrow) or activated mature (Splenic) T and B lymphocytes, measured following a 3.5 hour chase in the presence or absence of condensin I or II. **E.** Quantification of division efficiency, based on the % of BrdU$^+$ cells in G1 after 3.5 hours (n = 3 biological replicates from at least 2 independent experiments). Corresponding condensin depletion levels for each experiment are shown in Figure S3C **F**. Quantification of the effect of Ncaph or Ncaph2 degradation on cell division across cell types in panel E. For each cell type, division efficiency (panel E) in the vehicle only control condition was set to 100%, and the same parameter in IAA treated cells was expressed relative to this. Asterisks represent p-values from paired t-tests *** = $p < 0.01$, ** = $p < 0.05$, * = $p < 0.1$

Figure S3: Supplement to Figure 5.
A. The % of cells engaged in DNA replication (BrdU+) is not significantly different following acute depletion of Ncaph or Ncaph2. Each point shows the average % of cells incorporating BrdU following a 30 minute pulse following 2 hours of culture in 500μM IAA or vehicle, measured by flow cytometry. Bone marrow B cells required an extra hour of IAA treatment (3h total) to achieve robust depletion. Experimental schematic is shown in Figure 5A **B.** Acute depletion of Ncaph or Ncaph2 does not induce the DNA damage marker ɣH2AX in interphase cells undergoing DNA replication. Each point represents the average fluorescence intensity from at least 1000 single CD8$^+$ thymocytes single cells with DNA content between 2N and 4N (presumed to be in S phase). * indicates significant differences at $p < 0.05$ based on 2-tailed unpaired t-tests. Positive control wildtype cells were treated with 500μM hydroxyurea for 3 hours to induce replication fork collapse. **C**. Mean depletion levels of Ncaph and Ncaph2 proteins in the BrdU pulse chase experiments shown in Figure 5. Clover was quantified by flow cytometry in S/G2/M cells at the start (0hrs) and end (3.5hrs) of the chase period, with the +IAA value expressed as a % of vehicle only control after correcting for background autofluorescence. Where mean Clover fluorescence was lower than autofluorescence in the +IAA condition, a mean value of 0% was assigned. **D.** Reduced proliferation in peripheral B cells following acute degradation of Ncaph or Ncaph2, measured by Cell Trace flow cytometry assays. Contour plots show Cell Trace dye dilution via cell division following stimulation with LPS + IL4 for 48 hours in the continuous presence of 500μM IAA. Condensin-AID:Clover signal is shown on the y-axis to visualise degradation.

Figure 6: Rapid degradation of endogenous tagged proteins in living mice
A. (Top) I.P. injection time course to test protein degradation *in vivo*. Each mouse received a single injection of IAA solution (100mg/kg), or vehicle. (bottom). Boxplots show the extent of targeted protein degradation in >1000 S/G2/M CD8$^+$ thymocytes harvested 1 or 2 hours following auxin injection, measured by flow cytometry. % protein remaining was calculated as described in the Figure 2 legend. Boxes indicate the boundaries of upper and lower quartiles and whiskers show the range. Data are from 3 biological replicate injections performed over at least two independent experiments. **B**. Proteome quantification by mass spectrometry analysis of MACS-purified CD8$^+$ thymocytes. n = 3 animals per condition. **C.** Protein degradation and recovery following a single I.P. injection. Data are presented as described for panel A, except mice were heterozygous for the *Ncaph2$^{AID:Clover}$* allele. **D.** Schematic illustration of experimental workflow for protein degradation in E10.5 embryos. **E.** Example image from whole mount immunofluorescence performed on E10.5 embryo cryosections, stained with DAPI, anti-GFP-647 nanobooster (detecting Ncaph-AID:Clover) and anti-Cdh1. Anti-GFP signal was quantified within 5 Cdh1$^+$ regions of interest (ROI) per embryo, which were selected based solely on the Cdh1 staining pattern. To enable Cdh1 localisation and ROIs to be visualised, the anti-GFP-647 channel is not shown in this panel. Images were captured at 40X magnification, scale bar = 800μm **F.** Example ROI's from Cdh1$^+$ stained tissue on which target protein quantification was performed. To visualise degradation, only the Ncaph-AID:Clover channel is shown. Scale bar = 10μm **G.** Quantification of degradation efficiency in Cdh1$^+$ embryonic cells. Mean pixel intensity was

first calculated from 5 Cdh1^{+} regions in Ncaph$^{AID:Clover/AID:Clover}$ Rosa26$^{Tir1/Tir1}$ embryos from mothers injected with either IAA or vehicle, and non-fluorescent negative control embryos (n = 1 embryo each). The mean pixel intensity value from negative control ROIs was set to 0%, and the mean value from vehicle-only ROIs to 100%. Mean pixel intensity values for each ROI from vehicle and IAA-exposed embryos were then plotted on this scale. Negative values were set to 0%.

Figure S4: Supplement to Figure 6

A. Boxplots quantify the extent of targeted protein depletion in CD8^{+} thymocytes from *Ncaph$^{AID:Clover/+}$Rosa26^{Tir1}* animals injected with IAA at increasing dose. % protein remaining was calculated as described in the legend for Figure 2. Boxes show the boundaries of upper and lower quartiles and whiskers show the range. Where negative values were observed, a value of 0% was assigned. N = 1 per condition. **B.** A panel of liver function tests performed on plasma collected post-mortem from adult mice (n = 3 per condition) 2 hours or 72 hours after I.P. injection with IAA (100mg/kg) or vehicle. No significant differences ($p < 0.05$) were detected in unpaired two-tailed t-tests. ALP; Alkaline Phosphatase, AST; Aspartate Transaminase, ALT; Alanine transaminase. **C.** I.P. injection time course to test protein degradation in CD19^{+} bone marrow cells *in vivo.* Data were captured, analysed and presented as described in Figure 6A.

Figure S5: Supplement to Figure 6

A. Immunofluorescence on cryosections from small intestine of an *Ncaph$^{AID/AID}$ Rosa26$^{Tir1/Tir1}$* adult, fixed following 2 hour exposure to IAA *in vivo* (100mg/kg, I.P.). Scale bar 10μm. Ncaph degradation was quantified specifically within DAPI-stained regions of mitotic (ph3S10^{+}) cells, but can also be observed in the vast majority of interphase cells. Arrows show the position of an IAA-unresponsive cell. **B.** Different levels of Ncaph degradation observed in CD8^{+} thymocytes and Ter119^{+} erythroblasts from a single animal 2 hours following I.P. injection of IAA. **C.** Different levels of Ncaph degradation in CD19^{+} B cell precursors and Ter119^{+} erythroblasts following IAA treatment from the same *ex vivo* short-term bone marrow culture. In panels B & C, boxes show the boundaries of upper and lower quartiles and whiskers show the range of degradation values for >1000 S/G2/M cells, calculated as described in the legend for Figure 2. **D.** Immunofluorescence on cryosections from fixed adult testes (*Ncaph$^{AID/AID}$ Rosa26$^{Tir1/Tir1}$*) shows little if any target protein degradation. Yellow boxes in the upper panel show zoomed regions in the lower panel. Upper scale bar = 15μm, Lower scale bar = 10μm.

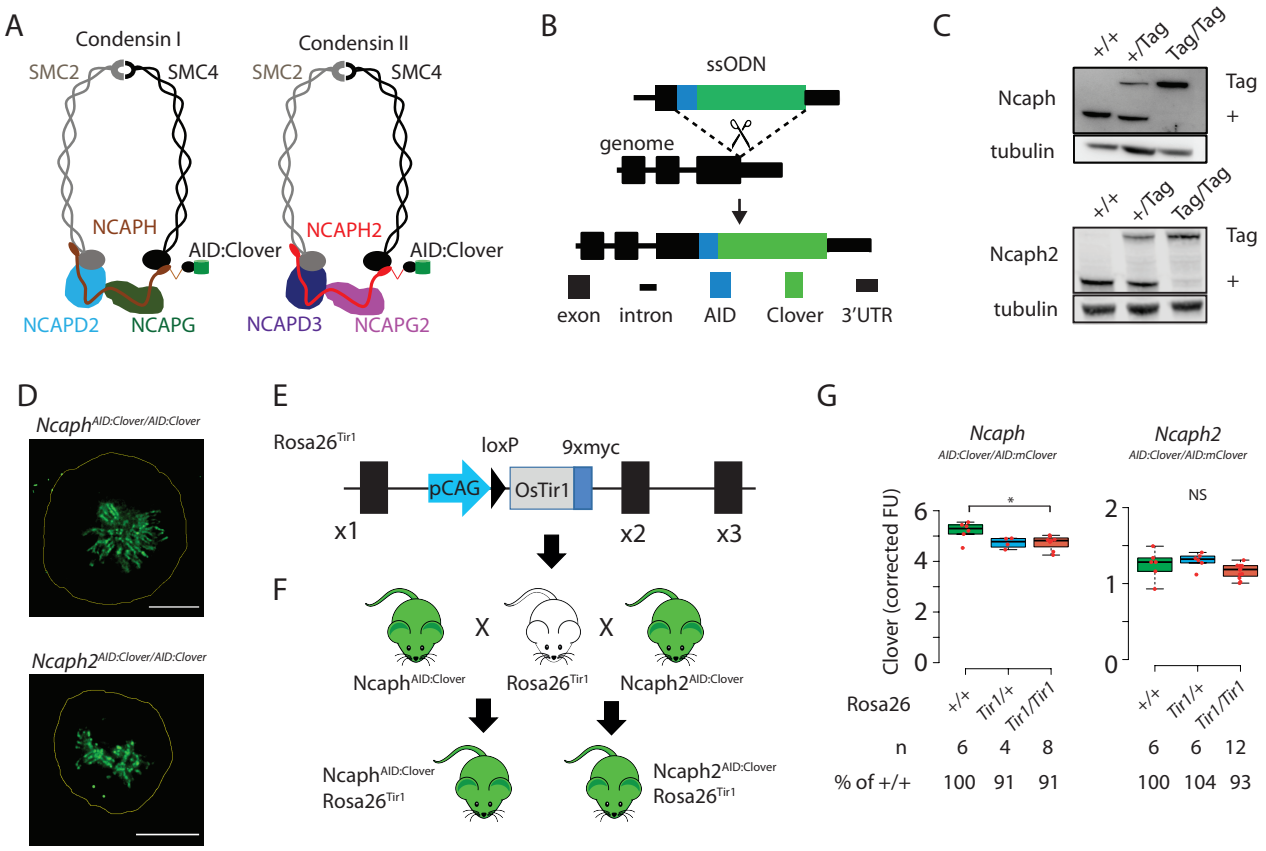

Figure 1: Mouse models for auxin-inducible degradation of condensin proteins

A. Schematic diagrams showing the subunit composition of condensin I and II complexes with C-terminal AID:Clover. The kleisin subunits of condensin I and II are Ncaph and Ncaph2, respectively. **B.** CRISPR-Cas9 strategy for integrating mClover cassettes at the Ncaph and Ncaph2 loci using long single stranded deoxyoligonucleotides (ssODN) to generate *Ncaph*$^{AID:Clover}$ and *Ncaph2*$^{AID:Clover}$ alleles. Full details and sequences for the integrated cassettes are given in Appendix S1. **C**. Western blots prepared from thymic whole cell protein extract were probed with antibodies recognising endogenous Ncaph or Ncaph2, with tubulin as a loading control. '+' indicates wildtype allele, 'tag' indicates AID:Clover. **D.** Immunofluorescence imaging of mitotic murine embryonic fibroblast lines derived from *Ncaph*$^{AID:Clover/AID:Clover}$ and *Ncaph2*$^{AID:Clover/AID:Clover}$ embryos. Scale bar = 5 μm. **E.** Schematic diagram showing the Rosa26^{Tir1} allele. Details on how this allele was generated are in Figure S1D and the materials and methods. **F.** Breeding scheme to combine endogenously-tagged *Ncaph* and *Ncaph2* alleles with *Rosa26*^{Tir1}. **G.** Clover fluorescence was measured by flow cytometry in primary S/G2/M thymocytes (gated on DNA content, n > 1000 cells/sample) from mice homozygous for AID:Clover-tagged target proteins, in combination with 0, 1 or 2 alleles of the Rosa26^{Tir1} transgene. Cells were not subjected to IAA treatment. Boxplots show background-corrected mean fluorescence values from (n) biological replicate samples. * indicates a significant ($p<0.05$) difference between genotypes (one-way ANOVA with Tukey HSD test, $p < 0.05$). NS: not significant.

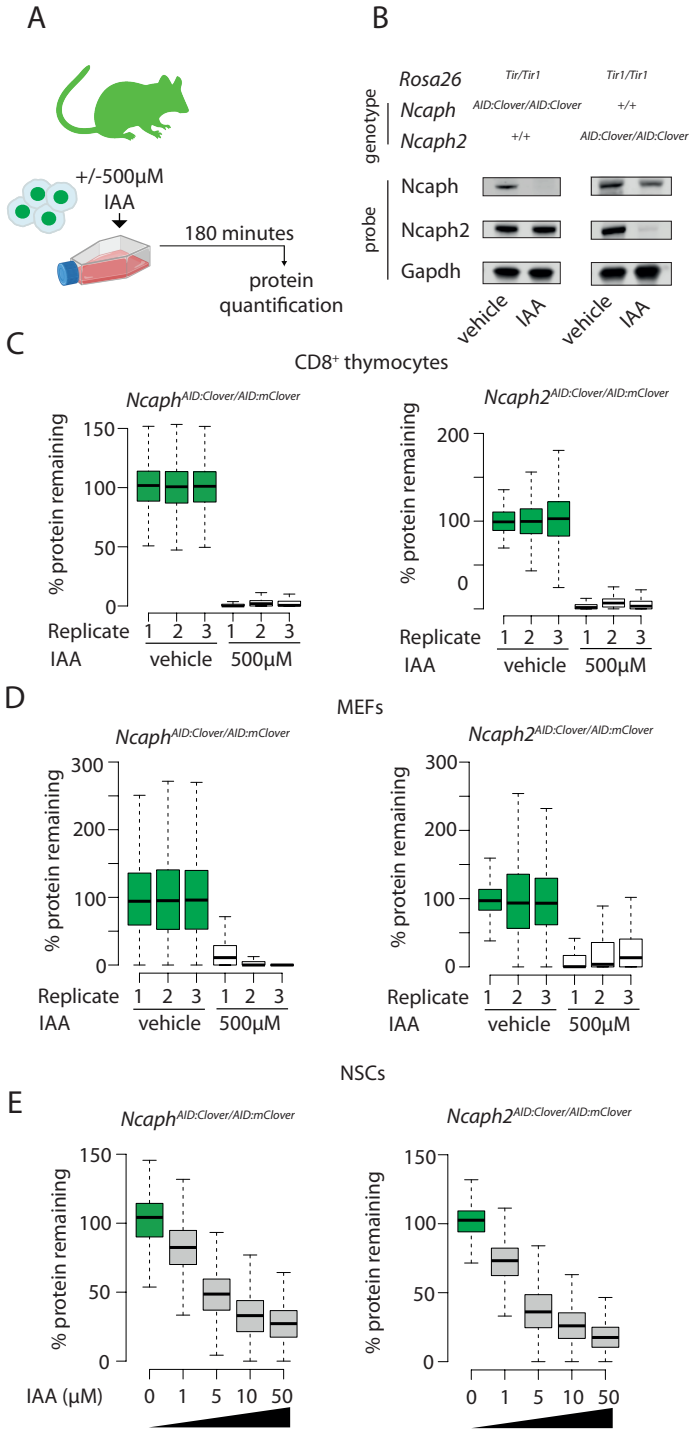

Figure 2: Rapid and titratable degradation of endogenous *Ncaph* and *Ncaph2* in primary cells

A. Schematic illustration of experiments designed to test targeted degradation of condensin subunits in primary cells. **B.** Western blots prepared from thymus whole cell extract and probed with polyclonal antibodies against Ncaph, Ncaph2, or a Gapdh loading control. Robust tag-dependent degradation of target proteins is clearly evident after 3 hours of auxin treatment. **C & D.** Boxplots quantify the extent of targeted protein depletion following IAA treatment (500μM for 3 hours), measured by flow cytometry in primary CD8⁺ thymocytes (C) and embryonic fibroblasts (D). n = 3 biological replicates from at least 2 independent experiments, with degradation measured in over 1000 S/G2/M cells in each case. To calculate % protein remaining, the background corrected fluorescence value of each cell was expressed as a percentage of the mean fluorescence value for all cells in the vehicle-only condition. Boxes show the boundaries of upper and lower quartiles and whiskers show the range. Where negative values were observed (e.g. in MEFs due to variable autofluorescence between lines), a value of 0% was assigned. **E.** Titration of target protein levels in primary neural stem cells treated with different IAA concentrations for 2 hours. Boxplots were generated as described for panels C&D.

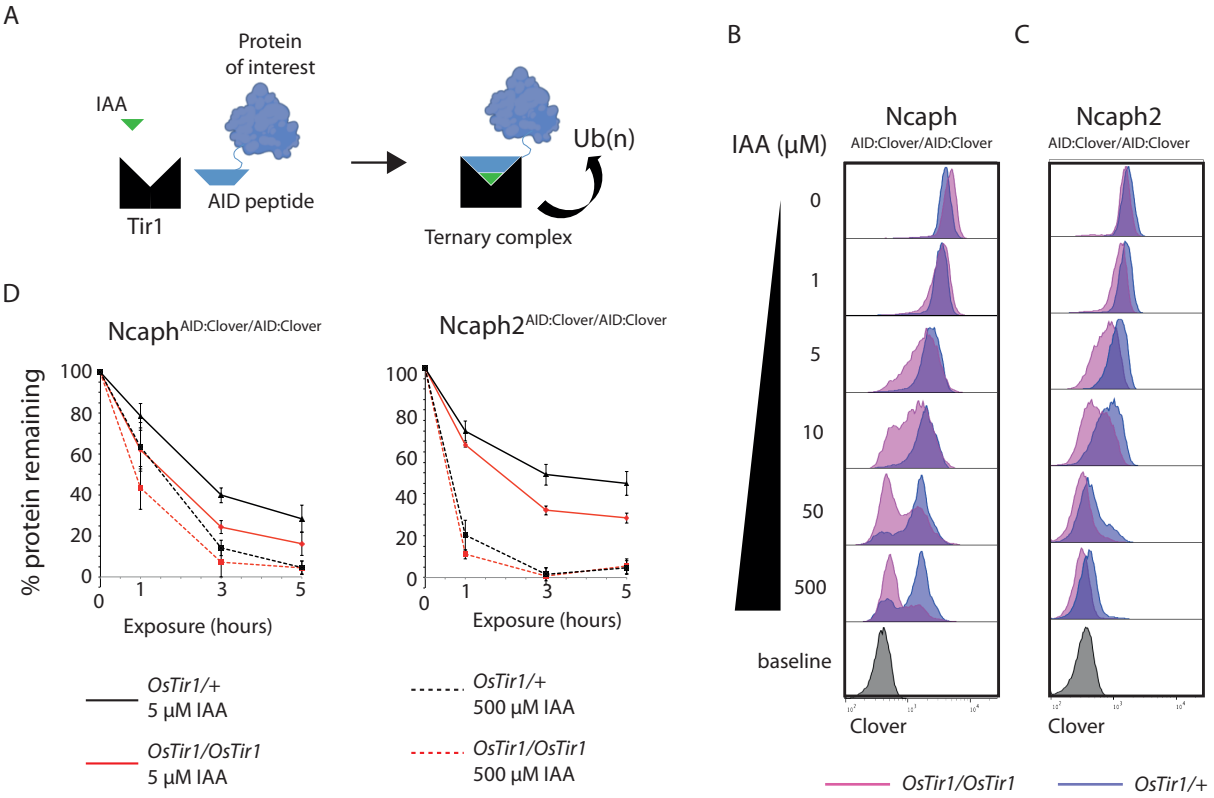

Figure 3: Tir1 dosage determines degradation kinetics of AID-tagged proteins.
A. Schematic diagram illustrates the assembly of the Tir1 substrate receptor protein, IAA ligand and AID tagged target protein-of-interest into a ternary complex necessary for target protein ubiquitination via SCF^{Tir1}, and degradation. **B & C**. Histograms show the distribution of Clover expression levels, measured by flow cytometry in S/G2/M thymocytes cultured for 2 hours *ex vivo* in the presence of different IAA concentrations. Thymocytes were isolated from animals homozygous for either (B) $Ncaph^{AID:Clover}$ or (C) $Ncaph2^{AID:Clover}$ alleles in combination with either one (dark purple) or two (light purple) alleles of $Rosa26^{Tir1}$. Equivalent data from animals heterozygous for AID-tagged alleles is shown in Figure S3. **D.** Comparison of depletion kinetics in the presence of one (black) versus two (red) alleles of the Tir1 transgene at low (solid line) versus high (dashed line) ligand concentrations (n = 3 biological replicate samples). Each experiment in panels B – D used data from at least 1000 S/G2/M thymocytes, gated on DNA content. In panel D, the mean background-corrected fluorescence value for each cell population is expressed as a percentage of the mean background-corrected fluorescence value for the vehicle only condition.

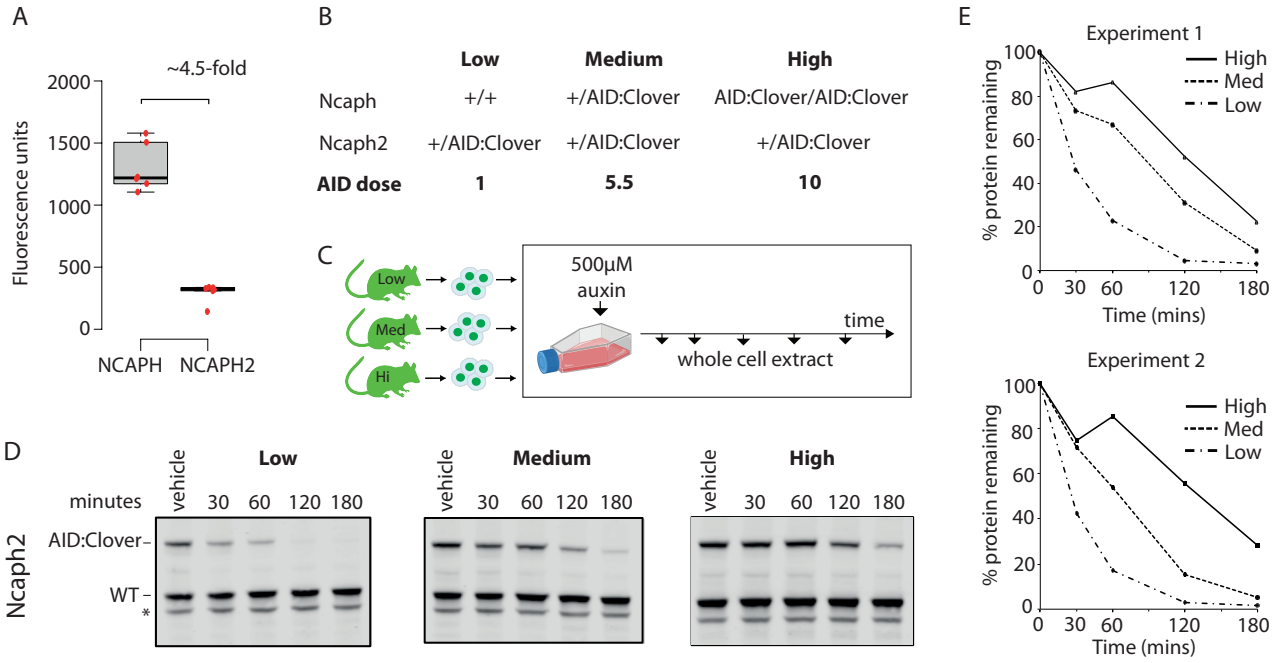

Figure 4: Dosage of AID-tagged proteins controls depletion kinetics

A. The relative expression of Ncaph and Ncaph2 (n = 6 biological replicates each) in S/G2/M thymocytes, based on flow cytometric Clover fluorescence measurements in > 1000 cells. **B**. Table showing the relative total dose of AID tagged proteins in mice heterozygous for *Ncaph2*$^{AID:Clover}$ in combination with either 0 (Low), 1 (Medium) or 2 (High) alleles of *Ncaph*$^{AID:Clover}$. Relative AID dose is calculated based on data in panel A. **C.** Schematic showing the time course for auxin treatment of primary thymocytes in panels D&E. **D.** Western blots probed with a polyclonal antibody against Ncaph2. Tagged protein (upper band) is degraded, whereas wildtype protein (lower band) is not. * indicates non-specific band. **E**. Quantification of Ncaph2-AID:Clover depletion in the presence of low, medium or high overall AID-tagged protein dose. Density of the AID:Clover band (see panel D) was first measured relative to the corresponding wildtype allele (bottom) as an internal control. The AID:WT ratio in the vehicle only control was set at 100% and IAA treatment conditions were then calculated relative to this value. Data from two independent experiments are presented.

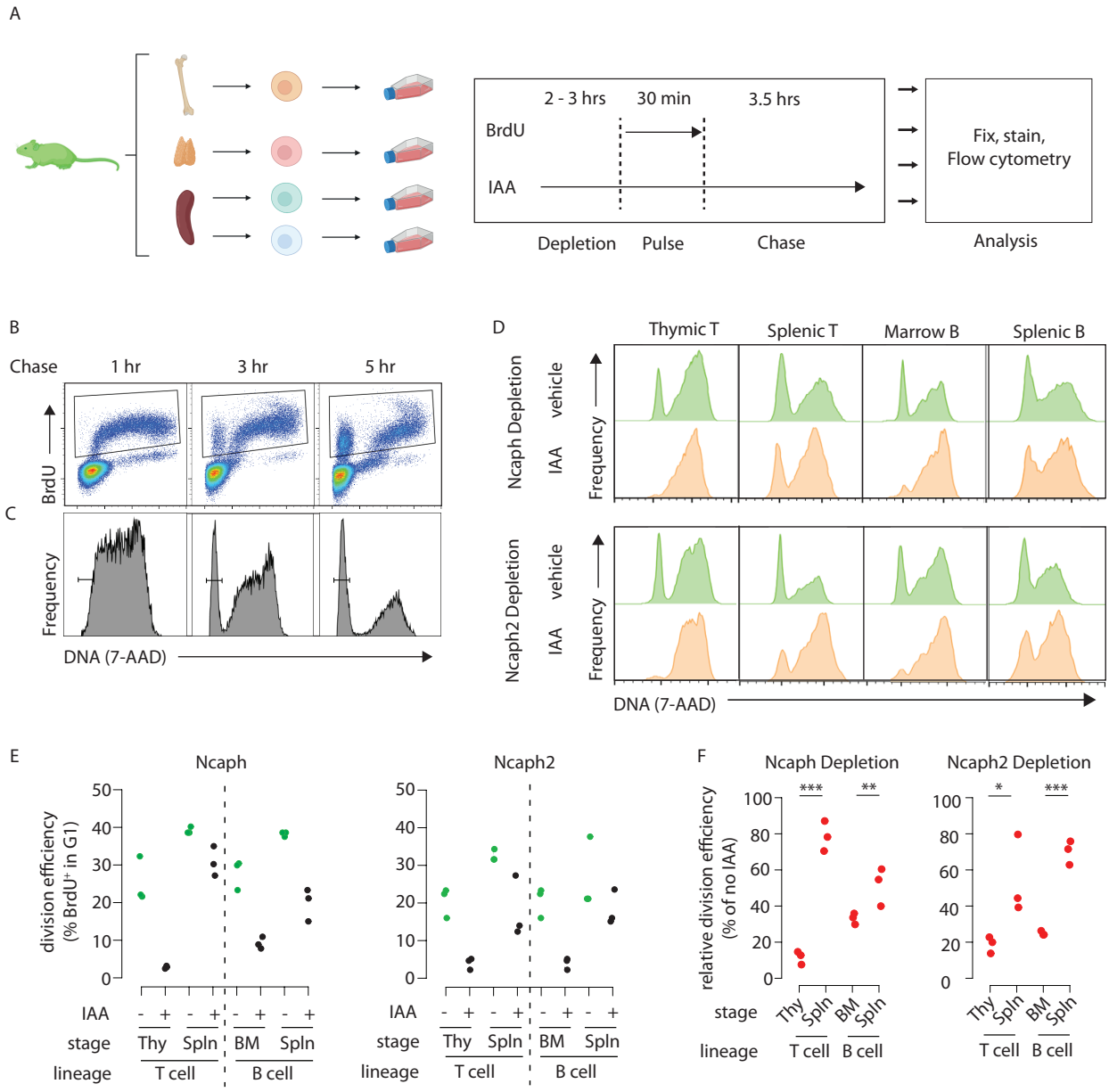

Figure 5: Dynamic changes in condensin dependency during lymphocyte differentiation

A. Chronological representation of the BrdU pulse chase assay to measure the efficiency of cell division in primary cell types cultured *ex vivo*. Lymphocyte isolation and culture protocols are detailed in the materials and methods. Quantifying the % of $BrdU^+$ cells (**B**) that complete mitosis and halve their DNA content (**C**) allows the efficiency of a single cell division to be quantified under normal or acute condensin deficient conditions. The appearance of $BrdU^+G1$ cells can be seen at 3 and 5 hours. **D.** Representative DNA content profiles, gated on $BrdU^+$ as shown in panel B, from cycling early (thymic / marrow) or activated mature (Splenic) T and B lymphocytes, measured following a 3.5 hour chase in the presence or absence of condensin I or II. **E.** Quantification of division efficiency, based on the % of $BrdU^+$ cells in G1 after 3.5 hours (n = 3 biological replicates from at least 2 independent experiments). Corresponding condensin depletion levels for each experiment are shown in Figure S3C **F**. Quantification of the effect of Ncaph or Ncaph2 degradation on cell division across cell types in panel E. For each cell type, division efficiency (panel E) in the vehicle only control condition was set to 100%, and the same parameter in IAA treated cells was expressed relative to this. Asterisks represent p-values from paired t-tests *** = $p < 0.01$, ** = $p < 0.05$, * = $p < 0.1$

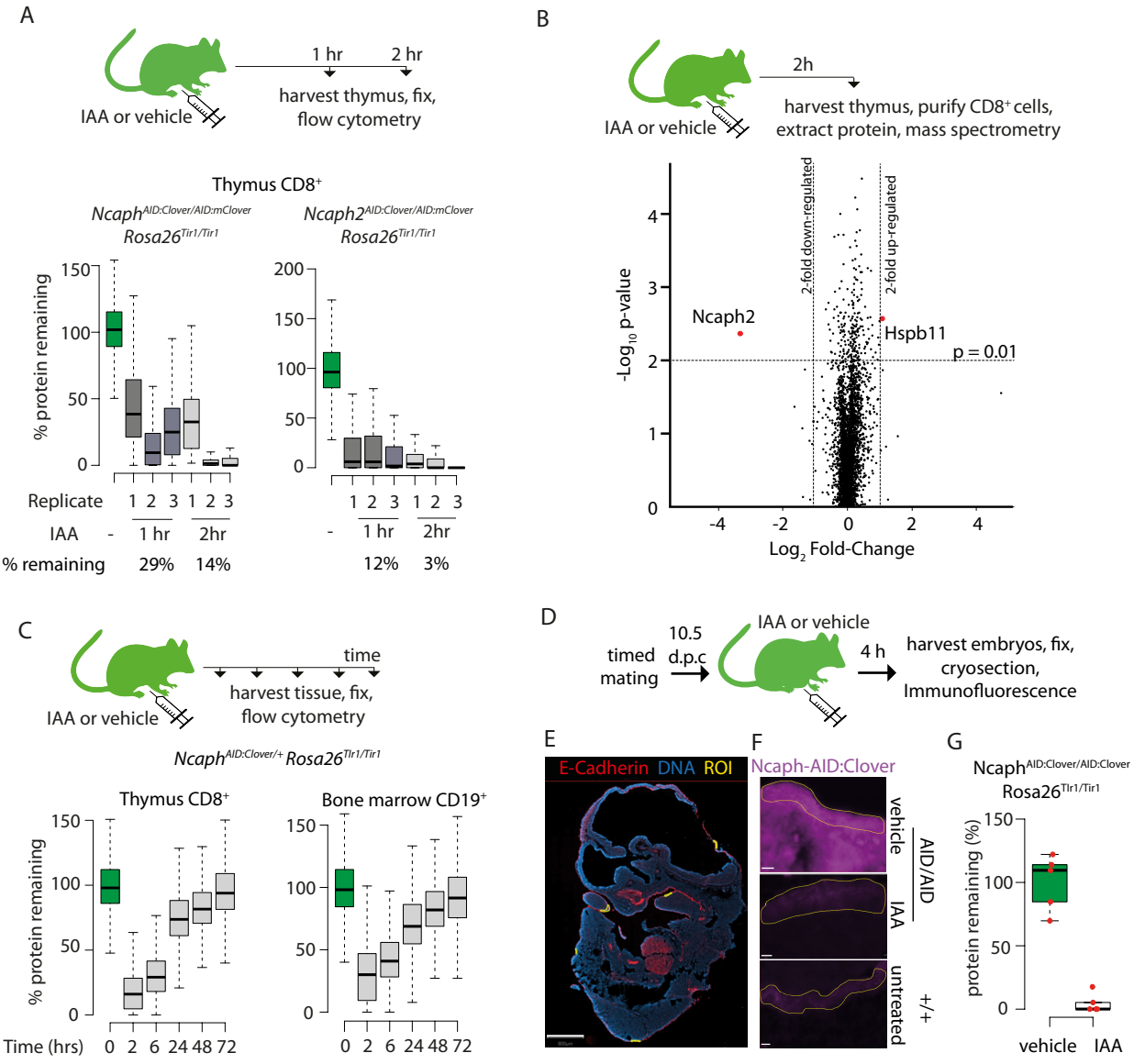

Figure 6: Rapid degradation of endogenous tagged proteins in living mice

Legend on next page

Figure 6: Rapid degradation of endogenous tagged proteins in living mice

A. (Top) Schematic illustration of an I.P. injection time course to test protein degradation *in vivo*. Each mouse received a single injection of IAA solution (100mg/kg), or vehicle. (bottom) Boxplots show the extent of targeted protein degradation in >1000 S/G2/M $CD8^+$ thymocytes harvested 1 or 2 hours following auxin injection, measured by flow cytometry. % protein remaining was calculated as described in the Figure 2 legend. Boxes indicate the boundaries of upper and lower quartiles and whiskers show the range. Data are from 3 biological replicate injections performed over at least two independent experiments. **B**. Proteome quantification by mass spectrometry analysis of MACS-purified $CD8^+$ thymocytes. n = 3 animals per condition. **C.** Protein degradation and recovery following a single I.P. injection. Data are presented as described for panel A, except mice were heterozygous for the *Ncaph2*$^{AID:Clover}$ allele. **D.** Schematic illustration of experimental workflow for protein degradation in E10.5 embryos. **E.** Example image from whole mount immunofluorescence performed on E10.5 embryo cryosections, stained with DAPI, anti-GFP-647 nanobooster (detecting Ncaph-AID:Clover) and anti-Cdh1. Anti-GFP signal was quantified within 5 $Cdh1^+$ regions of interest (ROI) per embryo, which were selected based solely on the Cdh1 staining pattern. To enable Cdh1 localisation and ROIs to be visualised, the anti-GFP-647 channel is not shown in this panel. Images were captured at 40X magnification, scale bar = 800μm **F.** Example ROI's from $Cdh1^+$ stained tissue on which target protein quantification was performed. To visualise degradation, only the Ncaph-AID:Clover channel is shown. Scale bar = 10μm **G.** Quantification of degradation efficiency in $Cdh1^+$ embryonic cells. Mean pixel intensity was first calculated from 5 $Cdh1^+$ regions in Ncaph$^{AID:Clover/AID:Clover}$ Rosa26$^{Tir1/Tir1}$ embryos from mothers injected with either IAA or vehicle, and non-fluorescent negative control embryos (n = 1 embryo each). The mean pixel intensity value from negative control ROIs was set to 0%, and the mean value from vehicle-only ROIs to 100%. Mean pixel intensity values for each ROI from vehicle and IAA-exposed embryos were then plotted on this scale. Negative values were set to 0%.

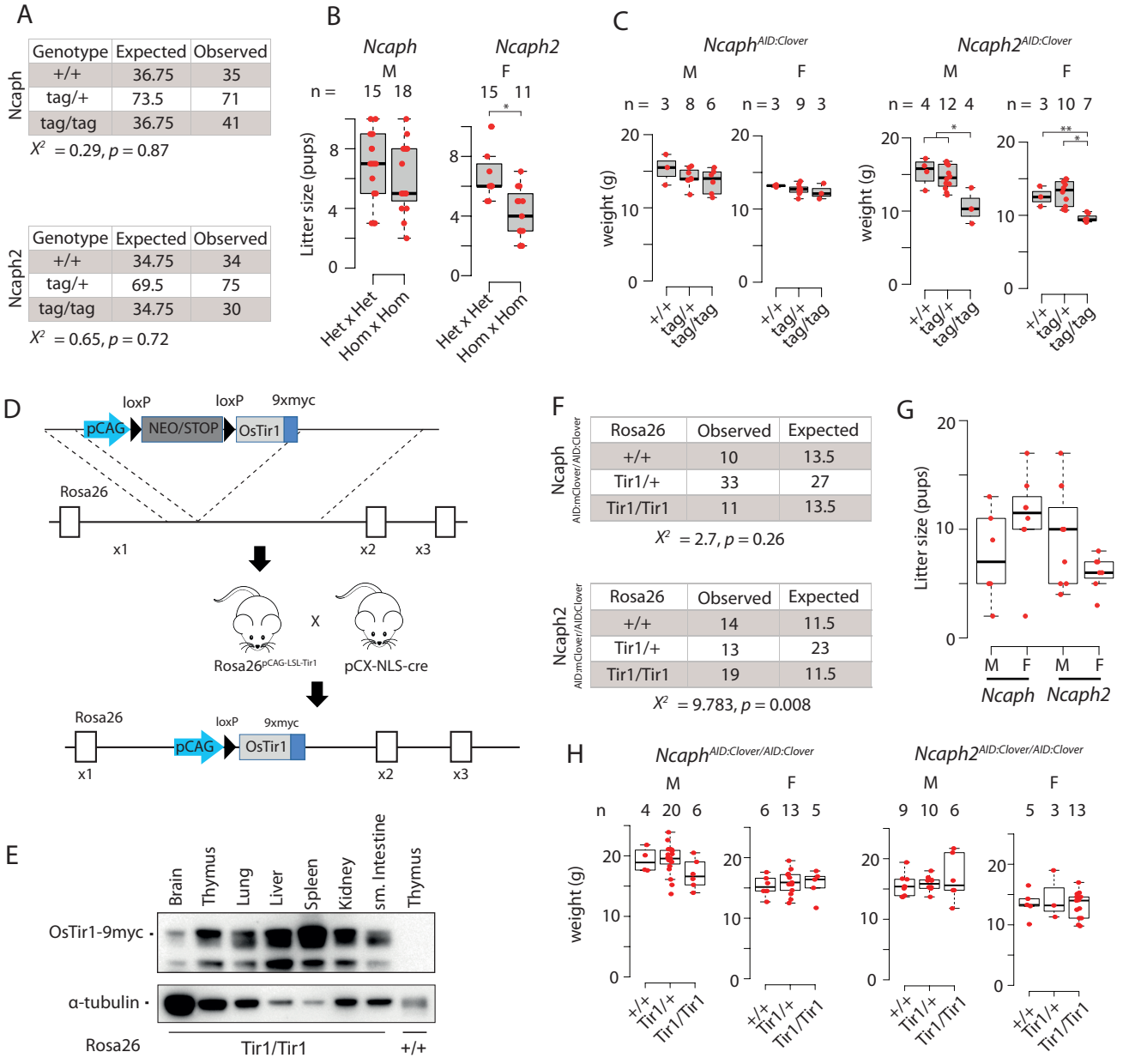

Figure S1: Supplement to Figure 1

A. Observed and expected genotype frequencies among 28 day-old animals generated from heterozygous crosses for each AID:Clover transgene (tag). Chi-squared tests revealed no significant deviation from expected mendelian frequencies. **B.** Litter sizes from matings between animals heterozygous versus homozygous for each AID:Clover transgene. * indicates significant difference at $p < 1 \times 10^{-3}$ from unpaired two-tailed t-tests **C.** Weight of pups at 28 days post-partum from crosses between parents heterozygous for the AID:Clover transgene (tag/+). M = male, F = female. * indicates significant differences between genotypes at $p < 0.01$, ** at $p < 0.05$ from one-way ANOVA with Tukey's HSD posthoc test. **D.** Schematic illustrating the derivation of $Rosa26^{Tir1}$ via a $Rosa26^{LSL\text{-}Tir1}$ intermediate. Breeding of $Rosa26^{pCAG\text{-}LSL}$ mice to pCX-NLS-cre caused germline deletion of the lox-stop-lox cassette to produce $Rosa26^{Tir1}$. **E.** Western blots of whole tissue extracts from $Rosa26^{Tir1/Tir1}$ or $Rosa26^{+/+}$ animals, probed with an anti-myc tag antibody (9B11). **F.** Observed and expected genotype frequencies among 28 day-old animals generated from crosses between parents homozygous for either *Ncaph*- or $Ncaph2^{AID:Clover}$ and heterozygous for $Rosa26^{OsTir1}$. Chi-squared tests revealed no significant deviation from expected mendelian frequencies of Rosa26 genotypes in the *Ncaph* background, and elevated frequencies of $Rosa26^{Tir1}$ homozygotes in the *Ncaph2* background. **G.** Litter sizes from any mating involving a male (M) or female (F) carrying $Rosa26^{Tir1}$ and either *Ncaph*- or $Ncaph2^{AID:Clover}$ alleles in the homozygous state, in combination with animals of various genotype. Because genotypes of the other animal in each mating differed between conditions, these data show simply that breeding from double homozygous transgenic mice is possible and are not suitable to quantify fertility across conditions. **H.** Weight of pups at 28 days post-partum. Differences between Tir1 genotypes were not significant at $p < 0.05$ in one-way ANOVA tests. M = male, F = female.

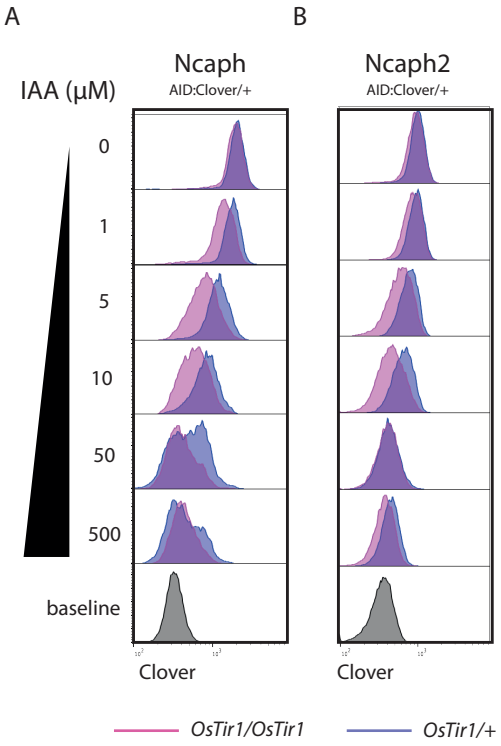

Figure S2: Supplement to Figure 3

A. Histograms show the distribution of Clover expression levels in >1000 S/G2/M thymocytes, cultured for 2 hours ex vivo in the presence of different IAA concentrations. Thymocytes were isolated from animals heterozygous for either (**A**) *Ncaph*$^{AID:Clover}$ or (**B**) *Ncaph2*$^{AID:Clover}$ alleles in combination with either one (dark purple) or two (light purple) alleles of Rosa26^{Tir1}.

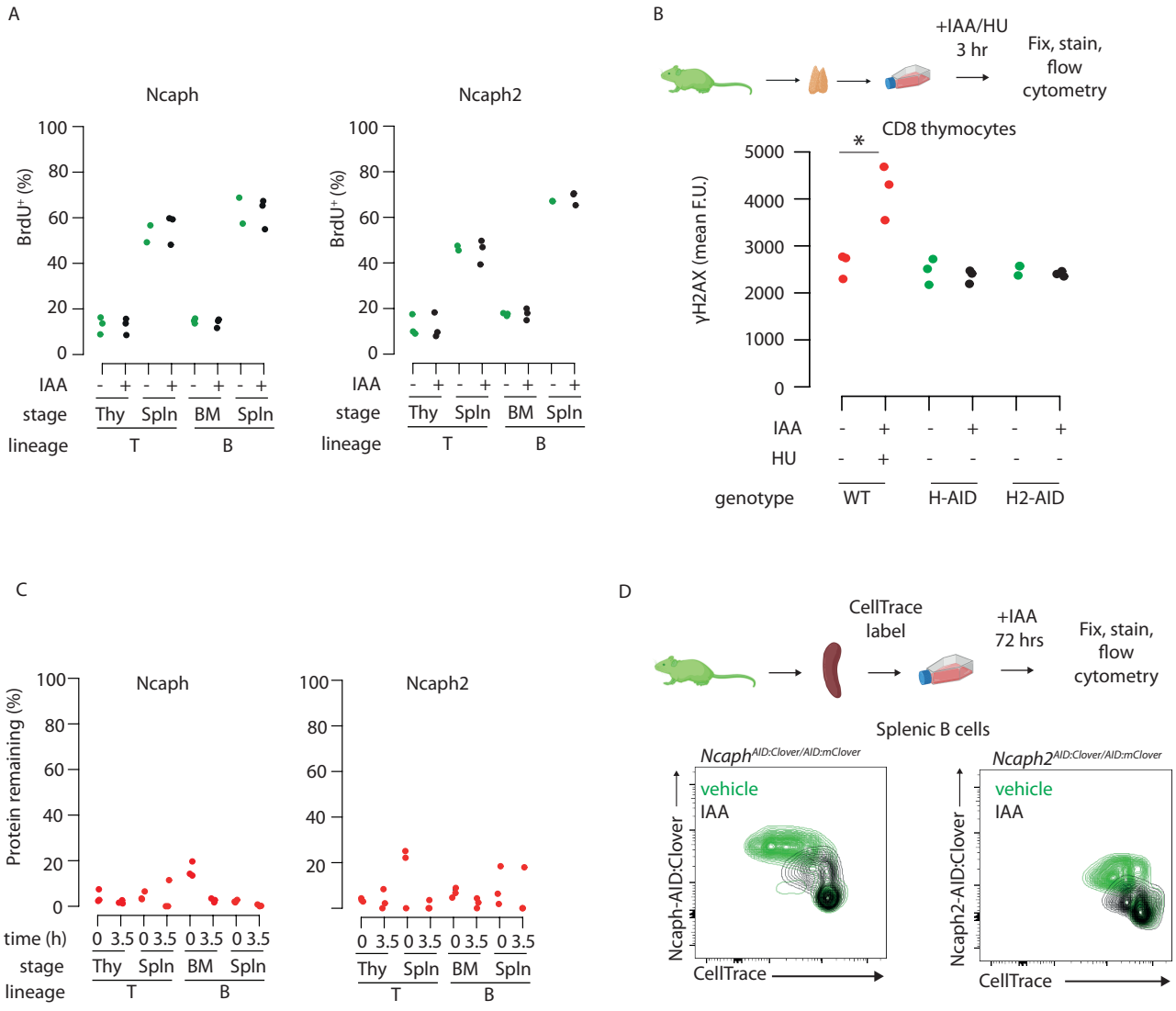

Figure S3: Supplement to Figure 5.

A. The % of cells engaged in DNA replication (BrdU+) is not significantly different following acute depletion of Ncaph or Ncaph2. Each point shows the average % of cells incorporating BrdU following a 30 minute pulse following 2 hours of culture in 500μM IAA or vehicle, measured by flow cytometry. Bone marrow B cells required an extra hour of IAA treatment (3h total) to achieve robust depletion. Experimental schematic is shown in Figure 5A **B.** Acute depletion of Ncaph or Ncaph2 does not induce the DNA damage marker γH2AX in interphase cells undergoing DNA replication. Each point represents the average fluorescence intensity from at least 1000 single $CD8^+$ thymocytes single cells with DNA content between 2N and 4N (presumed to be in S phase). * indicates significant differences at $p < 0.05$ based on 2-tailed unpaired t-tests. Positive control wildtype cells were treated with 500μM hydroxyurea for 3 hours to induce replication fork collapse. **C**. Mean depletion levels of Ncaph and Ncaph2 proteins in the BrdU pulse chase experiments shown in Figure 5. Clover was quantified by flow cytometry in S/G2/M cells at the start (0hrs) and end (3.5hrs) of the chase period, with the +IAA value expressed as a % of vehicle only control after correcting for background autofluorescence. Where mean Clover fluorescence was lower than autofluorescence in the +IAA condition, a mean value of 0% was assigned. **D.** Reduced proliferation in peripheral B cells following acute degradation of Ncaph or Ncaph2, measured by Cell Trace flow cytometry assays. Contour plots show Cell Trace dye dilution via cell division following stimulation with LPS + IL4 for 48 hours in the continuous presence of 500μM IAA. Condensin-AID:Clover signal is shown on the y-axis to visualise degradation.

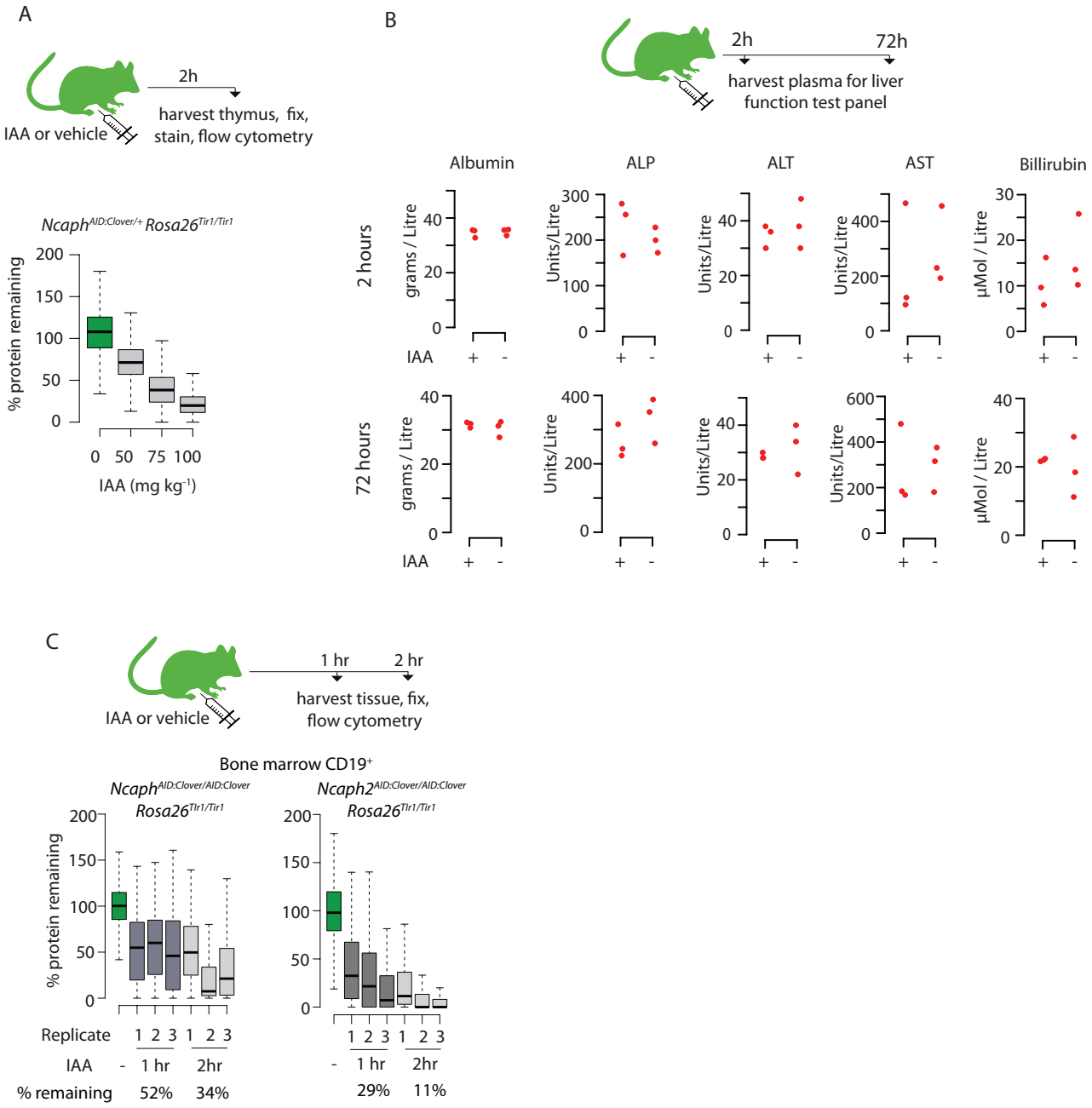

Figure S4: Supplement to Figure 6

A. Boxplots quantify the extent of targeted protein depletion in CD8$^+$ thymocytes from *Ncaph*$^{AID:Clover/+}$*Rosa26*^{Tir1} animals injected with IAA at increasing dose. % protein remaining was calculated as described in the legend for Figure 2. Boxes show the boundaries of upper and lower quartiles and whiskers show the range. Where negative values were observed, a value of 0% was assigned. N = 1 per condition. **B.** A panel of liver function tests performed on plasma collected post-mortem from adult mice (n = 3 per condition) 2 hours or 72 hours after I.P. injection with IAA (100mg/kg) or vehicle. No significant differences ($p < 0.05$) were detected in unpaired two-tailed t-tests. ALP; Alkaline Phosphatase, AST; Aspartate Transaminase, ALT; Alanine transaminase. **C.** I.P. injection time course to test protein degradation in CD19$^+$ bone marrow cells *in vivo.* Data were captured, analysed and presented as described in Figure 6A.

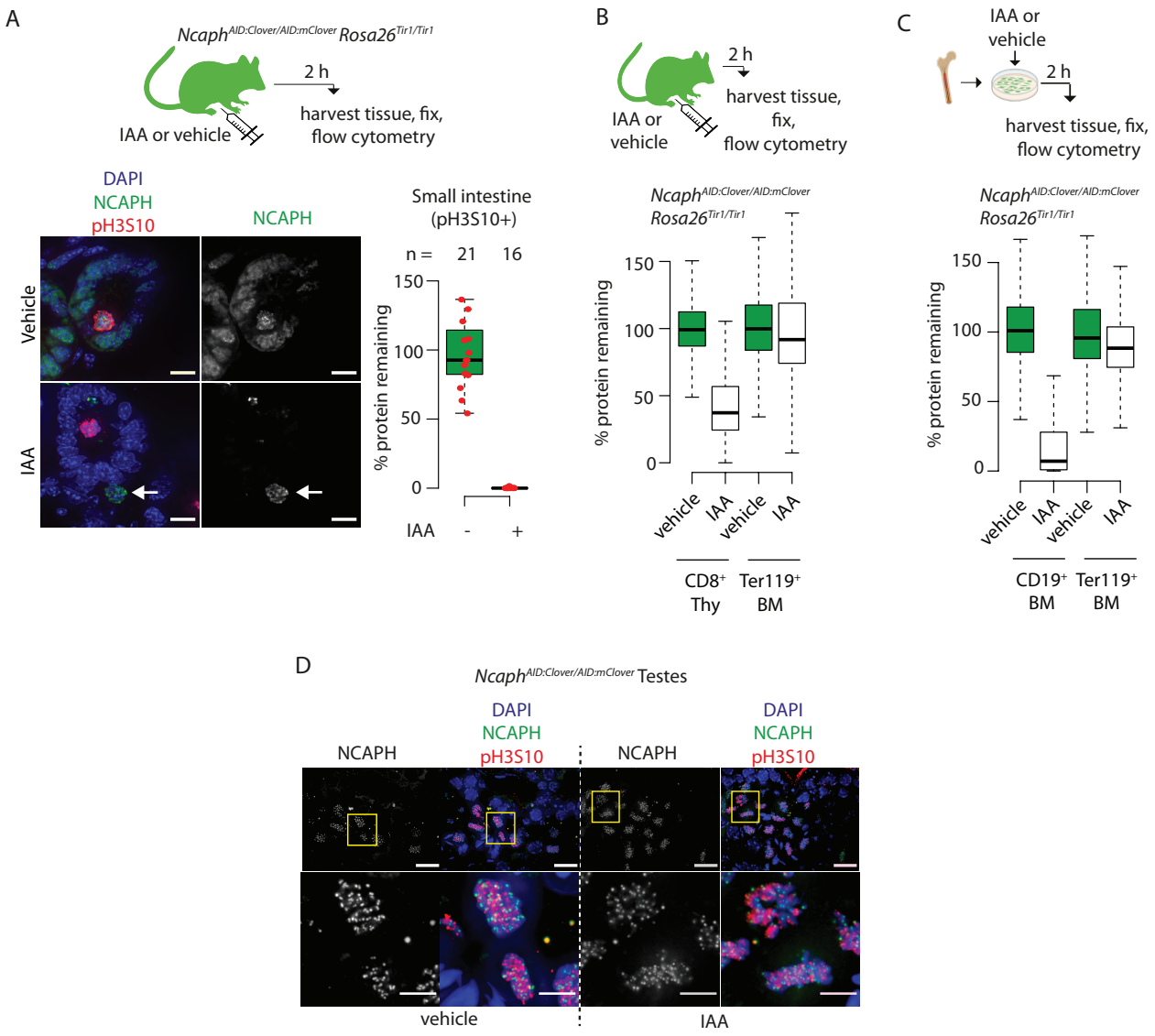

Figure S5: Supplement to Figure 6

A. Immunofluorescence on cryosections from small intestine of an *Ncaph*$^{AID/AID}$ *Rosa26*$^{Tir1/Tir1}$ adult, fixed following 2 hour exposure to IAA *in vivo* (100mg/kg, I.P.). Scale bar 10μm. Ncaph degradation was quantified specifically within DAPI-stained regions of mitotic (ph3S10^{+}) cells, but can also be observed in the vast majority of interphase cells. Arrows show the position of an IAA-unresponsive cell. **B.** Different levels of Ncaph degradation observed in CD8^{+} thymocytes and Ter119^{+} erythroblasts from a single animal 2 hours following I.P. injection of IAA. **C.** Different levels of Ncaph degradation in CD19^{+} B cell precursors and Ter119^{+} erythroblasts following IAA treatment from the same *ex vivo* short-term bone marrow culture. In panels B & C, boxes show the boundaries of upper and lower quartiles and whiskers show the range of degradation values for >1000 S/G2/M cells, calculated as described in the legend for Figure 2. **D.** Immunofluorescence on cryosections from fixed adult testes (*Ncaph*$^{AID/AID}$ *Rosa26*$^{Tir1/Tir1}$) shows little if any target protein degradation. Yellow boxes in the upper panel show zoomed regions in the lower panel. Upper scale bar = 15μm, Lower scale bar = 10μm.